1   **Two cowpea Rubisco activase isoforms for crop thermotolerance**

2   Armida Gjindali; Rhiannon Page; Catherine J. Ashton; Ingrid Robertson; Mike T. Page;

3   Duncan Bloemers; Peter D. Gould; Dawn Worrall; Douglas J. Orr; Elizabete Carmo-Silva

4   Lancaster Environment Centre, Lancaster University, Lancaster, LA1 4YQ, UK

5   Corresponding author email: e.carmosilva@lancaster.ac.uk

6

13

14   Summary

15   • A vital crop for sub-Saharan Africa, cowpea productivity is threatened by climate
16   change, including increased heatwave intensity, duration, and frequency. Rubisco
17   activase (Rca) is a key molecular chaperone that maintains Rubisco activity and due
18   to its thermal sensitivity is a key target for improving crop climate resilience.

19   • We identified and characterised four Rca isoforms in *Vigna unguiculata* (L.) Walp. cv.
20   IT97K-499-35 *in vitro*: Rca1β, Rca8α, Rca10α and Rca10β. Cowpea leaf and plant
21   growth traits were also investigated during a 5-day +10 °C heatwave that included
22   assessment of Rubisco and Rca activity in leaf extracts, and relative changes in the
23   abundance of the four Rca isoforms.

24   • Cowpea Rca10α and Rca10β had higher thermal maxima, broader thermal optima
25   and higher rates of ATP hydrolysis and Rubisco reactivation *in vitro*. In the absence
26   of water deficit, the heatwave caused only mild effects, including increases in leaf
27   temperature and expression of *Rca10*, small decreases in Rubisco activity and
28   activation state, and unaltered temperature response of Rubisco activation by Rca.

29   • The superior Rca10α and Rca10β isoforms offer the prospect of enhancing the
30   thermotolerance of cowpea and other crops in anticipation of more extreme future
31   heatwaves.

32

33   Keywords: Activase, cowpea, heat stress, photosynthesis, Rca, Rubisco, temperature
34   response, *Vigna unguiculata*.

35

Introduction

Changes in global temperatures including heatwave events pose significant threats to global food security (Moore *et al.*, 2021), making increased crop resilience against heat stress imperative (Song *et al.*, 2023). Regions closer to the equator, particularly sub-Saharan Africa, are the most vulnerable to rising temperatures (Harboure, 2024). Elevated temperatures can lead to decreased photosynthesis and plant growth (Hatfield & Prueger, 2011; Bagati *et al.*, 2021; Zahra *et al.*, 2023; Becker *et al.*, 2023). Cowpea (*Vigna unguiculata* (L.) Walp) is a major source of protein for populations in sub-Saharan Africa and, despite being adapted to a warm climate, it is still vulnerable to heat stress – even a 1 °C increase in night temperature can result in significant yield loss (Warrag & Hall, 1984; Gonçalves *et al.*, 2016; Mohammed *et al.*, 2024). Therefore, it is imperative to identify physiological and biochemical traits that confer thermotolerance in cowpea to develop heat resilient crops (Barros *et al.*, 2021).

Moderate heat stress, defined as temperatures up to 40 °C (Crafts-Brandner & Salvucci, 2000; Kumar *et al.*, 2009; Ara *et al.*, 2013), has a profound impact on plant photosynthesis, adversely affecting both the electron transport chain and the Calvin-Benson-Bassham (CBB) cycle (Chen *et al.*, 2022). Rubisco and chlorophyll leaf content also decline under moderate heat stress (Mathur *et al.*, 2014). Chlorophyll biosynthesis enzymes exhibit susceptibility to heat stress; however, the reduction in Rubisco content cannot be attributed to denaturation of Rubisco, as alterations in secondary structure are observed only at temperatures exceeding 45 °C (Li *et al.*, 2002; Mathur *et al.*, 2014). Increased temperatures enhance Rubisco carboxylation activity; but they also decrease Rubisco CO_2/O_2 specificity and the ratio of CO_2/O_2 solubilities, thereby increasing the proportion of oxygenation reactions leading to increased photorespiration (Hermida-Carrera *et al.*, 2016; Galmés *et al.*, 2016). Importantly, increased carbon loss through photorespiration does not fully account for the decrease in carbon assimilation during moderate heat stress, as the Rubisco activation state has been demonstrated to decrease under both photorespiratory and non-photorespiratory conditions during mild heat stress (Feller *et al.*, 1998; Crafts-Brandner & Law, 2000; Galmés *et al.*, 2016).

Numerous studies have demonstrated that Rubisco inactivation is one of the primary causes of reduced photosynthetic efficiency during moderate heat stress (Feller *et al.*, 1998; Crafts-Brandner & Law, 2000; Portis, 2003; Ristic *et al.*, 2009; Carmo-Silva *et al.*, 2015; Perdomo *et al.*, 2017; Wijewardene *et al.*, 2021; Scafaro *et al.*, 2023). To catalyse carboxylation or oxygenation, Rubisco catalytic sites require binding of CO_2 and Mg^{2+} as cofactors to form the active carbamylated Rubisco prior to binding the substrate ribulose 1,5-biphosphate (RuBP). Rubisco can become inactivated by the binding of inhibitory sugar phosphates to

72   carbamylated catalytic sites or by misfire products that cannot dissociate and maintain

73   catalytic sites in their closed, inactive conformation (Orr *et al.*, 2023). Inactivation can also

74   occur when RuBP binds to an uncarbamylated Rubisco catalytic site. Inhibited Rubisco

75   requires its molecular chaperone Rubisco activase (Rca) to restore its activity (Carmo-Silva

76   & Salvucci, 2013). Rca is a nuclear encoded protein that belongs to the AAA+ ATPases

77   superfamily (Hazra *et al.*, 2015) and, in its active multimeric form, exhibits two activities: ATP

78   hydrolysis and Rubisco reactivation (Bhat *et al.*, 2017; Serban *et al.*, 2018). Rca docks on

79   Rubisco's large subunit and, using ATP, performs conformational remodelling to release the

80   inhibitory compound, thus modulating Rubisco activity by facilitating the dissociation of

81   bound inhibitors. Elevated temperatures increase the frequency of Rubisco inactivation due

82   to higher concentrations of some inhibitory substrates (Salvucci & Crafts-Brandner, 2004, p.

83   20). Furthermore, although Rubisco is a relatively thermostable enzyme, Rca is thermolabile

84   and even a moderate increase in temperature results in loss of its activity (Crafts-Brandner &

85   Salvucci, 2000; Salvucci *et al.*, 2001).

86   Rca isoforms within a single species vary in their regulatory properties (Zhang & Portis,

87   1999; Carmo-Silva & Salvucci, 2013; Perdomo *et al.*, 2019; Scafaro *et al.*, 2019b). Many

88   species express two types of Rca isoforms: longer α isoforms (43-47 kDa) and shorter β

89   isoforms (41-43 kDa) that can be encoded either by individual genes or the same gene via

90   alternative splicing (Carmo-Silva *et al.*, 2015). Rca α isoforms contain a C-terminal extension

91   with two cysteine residues shown to form a disulfide bond which is regulated by thioredoxin-f

92   in *Arabidopsis* (Zhang & Portis, 1999). This regulatory mechanism links Rubisco activity with

93   alterations in the redox potential induced by environmental stimuli, such as high light (Zhang

94   *et al.*, 2002; Perdomo *et al.*, 2021). The redox regulation is species-specific, with

95   Solanaceae species such as tobacco (*Nicotiana tabacum* L.) and tomato (*Solanum*

96   *lycopersicum* L.) containing only the β Rca isoform that lacks the cysteine residues and the

97   redox regulation of the enzyme (Carmo-Silva & Salvucci, 2013). In species containing only

98   redox insensitive Rca, light regulation appears to be mediated by changes in the ADP/ATP

99   ratio of the chloroplast (Carmo-Silva & Salvucci, 2013).

100   In addition to variation in the number of genes and the isoforms they produce, the

101   expression and relative abundance of Rca isoforms vary among species and as a response

102   to temperature (Law & Crafts-Brandner, 2001; Wang *et al.*, 2010; Degen *et al.*, 2020;

103   Perdomo *et al.*, 2021). In rice (*Oryza sativa* L.) two Rca isoforms are produced via

104   alternative splicing and while Rca β is more abundant under optimal steady state conditions

105   (Wang *et al.*, 2010), heat stress induces upregulation of Rca α (Scafaro *et al.*, 2016). In

106   maize (*Zea mays* L.) the two isoforms derive from two genes *ZmRcaα* and *ZmRcaβ*

107   encoding an α (43 kDa) and a β (41 kDa) isoform respectively (Yin *et al.*, 2014). Under

108   optimal temperature conditions, the ZmRca β protein isoform is expressed in higher levels
109   than ZmRca α and both exhibit comparable diurnal variation in expression levels (Ristic *et*
110   *al.*, 2009). Jiménez *et al.* reported an increase in ZmRca α in seedlings exposed to higher
111   temperatures, however in more mature heat-treated plants this effect was not consistent
112   (Ristic *et al.*, 2009; Stainbrook *et al.*, 2024). In wheat (*Triticum aestivum* L.) there are two
113   *Rca* genes, one of which produces a β isoform while the other (*TaRca2*) is alternatively
114   spliced and produces both an α and a β isoform (Nagarajan & Gill, 2018). The Rca α/β ratio
115   changes when wheat is exposed to heat stress, suggesting that the relative abundance of
116   the different Rca isoforms is linked with the physiological response to heat stress (Warrag &
117   Hall, 1984; Crafts-Brandner & Salvucci, 2000). By contrast, in *Arabidopsis* the Rca isoform
118   ratio is not impacted by heat, with the α and β isoforms originating from alternative splicing
119   continuing to be expressed at a 1:1 ratio (Zhang & Portis, 1999). These species-specific
120   responses of Rca and Rubisco regulation to heat stress illustrate the need to investigate this
121   system directly in the crop of interest.

122   While the exact mechanism of Rca deactivation at high temperatures is still not fully
123   understood, it is evident that the optimum temperature range for Rca is species-specific and
124   in tune with the photosynthetic optimum (Scafaro *et al.*, 2016). Therefore, the temperature at
125   which Rca loses its activity depends on environmental acclimation; i.e., plants that grow at
126   high temperatures, such as cotton and agave, maintain Rca activity at higher temperatures
127   (Salvucci & Crafts-Brandner, 2004; Carmo-Silva & Salvucci, 2011; Scafaro *et al.*, 2016;
128   Shivhare & Mueller-Cajar, 2017). Rca thermotolerance also differs between closely related
129   species and among the native Rca isoforms within a plant species. The wild rice species
130   *Oryza australiensis* Domin and *Oryza meridionalis* Ng. contain thermostable Rca isoforms
131   that enable sustained high Rubisco activity and photosynthetic rate even at 45 °C (Scafaro
132   *et al.*, 2016, 2018). In rice, spinach and cotton, the α isoform exhibits higher thermostability
133   whereas in wheat, it is one of the two shorter β (TaRca1β) isoforms that is most
134   thermostable (Kurek *et al.*, 2007; Wang *et al.*, 2010; Keown & Pearce, 2014; Degen *et al.*,
135   2020). Increasing the thermostability of Rca is considered one of the most promising
136   strategies for increasing Rubisco activity and enhancing photosynthesis under elevated
137   temperature (Carmo-Silva *et al.*, 2015; Wijewardene *et al.*, 2021).

138   In this study we identified four Rca isoforms in cowpea encoded by three genes: *Rca1*, *Rca8*
139   and *Rca10*, with the latter producing two isoforms via alternative splicing. Characterisation of
140   their ATPase and Rubisco reactivation activities across a range of temperatures *in vitro*
141   revealed that the two Rca10 protein isoforms have higher thermal maxima and broader
142   thermal optima for both activities. We then examined the effect of moderate heat stress
143   during a 5-day heatwave at 38 °C (+10°C compared to control) on the expression and

144   abundance of Rca isoforms and subsequent impacts on Rubisco activation in the leaves of

145   young cowpea plants. Heat treatment resulted in decreased Rubisco activation state and

146   upregulation of *Rca8a* and *Rca10* gene expression, however the levels of *Rca10*, which

147   encodes both Rca10 isoforms, were consistently the lowest. Despite upregulation of the

148   more thermotolerant isoforms, the temperature profile of Rubisco reactivation by Rca in leaf

149   extracts remained unaltered in heat-treated plants. Leaf temperature increased by 6 °C

150   during the heatwave, reaching 32 °C, which is within the temperature range where Rca

151   activity is maintained above 70% of the maximum (T_{opt}) for all isoforms. We therefore

152   conclude that warm-adapted cowpea plants can cope with the mild heat stress induced by a

153   5-day heatwave at 38 °C in the absence of water deficit, which did not impair Rca function.

154   Overexpression of the most thermotolerant, yet least abundant, Rca isoforms in cowpea

155   could enable adaptation to leaf temperatures resulting from heatwaves that are more intense

156   or accompanied by water deficit, which are likely to occur in sub-Saharan Africa.

Materials and Methods

Gene identification

Cowpea *Rca* genes were identified by searching the cowpea genome (Phytozome 12, cowpea genome v1.1) using keywords and known Rca protein sequences from *Arabidopsis thaliana*, *Nicotiana tabacum*, and *Triticum aestivum* (Supporting Information Table S1)(Goodstein *et al.*, 2012; Lonardi *et al.*, 2019). This identified 3 genes for *Rca* in cowpea: *Vigun01g219300* (*Rca1*), *Vigun08g150700* (*Rca8*), and *Vigun10g051600* (*Rca10*). Alignment with known sequences and key conserved features of canonical Rcas allowed identification of the products of each gene, including cases where alternative splicing was present. Transit peptide sequences for each protein were identified by alignment to known Rca sequences (with known transit peptide locations). The analysis was repeated using the updated Phytozome 13 cowpea genome v1.2 and yielded identical Rca isoforms (Supporting Information Fig. S1). Of the various transcripts for each gene, some encode the exact same protein sequence and were grouped together, some lack one or more domains of the protein that are essential for function and were disregarded, and some are not expressed and were disregarded. This analysis of transcript sequences showed that *Rca1* encodes a 384 amino acid (aa) mature protein consistent with a β isoform. *Rca8* encodes a 419 aa α isoform and a 295 aa isoform that is shorter than a regular β isoform and unlikely to be functional as it lacks part of the α helical and the whole C terminal domain, which has been shown to be essential for both ATPase and Rubisco reactivation activity (Stotz *et al.*, 2011). *Rca10* encodes both a 419 aa α and a 382 aa β isoform by alternative splicing.

The cowpea *HSP20* (*Vigun06g052200*) gene, used as a heat stress marker, was identified as a homolog of the soybean *HSP20* (*Glyma.18g094600*) shown to be upregulated in two soybean cultivars exposed to heat stress (Song *et al.*, 2017). The Arabidopsis homolog (*At4G27670*) is also upregulated in heat stress (eFP Browser Stress Series, https://bar.utoronto.ca/)(Kilian *et al.*, 2007; Winter *et al.*, 2007). The *Glyma.18g094600* coding sequence was downloaded from SoyBase (https://legacy.soybase.org) and used to search the cowpea genome as above (Brown *et al.*, 2021).

Cloning of cowpea Rca and construction of *E. coli* expression vectors

Coding regions for the mature proteins of cowpea Rca1β, Rca8α, Rca10α and Rca10β were codon optimised for *E. coli, de novo* synthesised and subcloned into pUC57 (Kan^R) by Aruru Molecular Ltd. (Dundee, UK). A Golden Gate compatible *E.coli* expression vector was created from the pET His TEV LIC plasmid (a gift from Scott Gradia, Addgene plasmid #29653; http://n2t.net/addgene:29653; RRID:Addgene_29653). Ligation independent cloning was used to add a Golden Gate cassette taken from pICH47742 (part of the MoClo Toolkit

192　　that was a gift from Sylvestre Marillonnet, Addgene kit # 1000000044) into pET His TEV LIC,

193　　generating the new Golden Gate compatible pET His TEV GG plasmid (Weber *et al.*, 2011;

194　　Werner *et al.*, 2012). Cloning a coding region into this vector allows production of a target

195　　protein fused to an N-terminal histidine (His) tag that can be removed with TEV protease.

196　　PCR was used to add Golden Gate overhangs to the four optimised *Rca* sequences (see

197　　Supporting Information Table S2 for primers used). Golden Gate reactions (final volume 15

198　　µL) were performed with a 2:1 molar ratio of insert:plasmid and the following reagents (final

199　　concentration): 1× T4 DNA Ligase buffer, 0.1 mg mL^{-1} BSA, 1 mM ATP, 40 KU/mL T4 DNA

200　　Ligase, 2 KU/mL *Bsa* I. All reagents from NEB, except ATP (Promega). Reaction conditions

201　　were 30 cycles of [37 °C for 2 min followed by 16 °C for 3 min], 37 °C for 5 min, 80 °C for 10

202　　min, and 16 °C for 1 min. 5 µL of the reaction mix was used to transform *E. coli* DH5α cells.

203　　Resulting colonies were used to generate plasmid DNA for sequencing with primers T7F and

204　　T7R (Source Bioscience) to verify correct sequence including in-frame fusion of the coding

205　　region to the His tag.

Recombinant Rca expression and purification

207　　Expression constructs were used to transform BL21(DE3)pLysS *E. coli* competent cells

208　　(Invitrogen). PCR and sequencing were used to confirm the presence of the correct

209　　constructs in the BL21(DE3)plysS *E. coli* cells. Several cell lines were tested for each

210　　construct to identify the cell strains with the highest expression levels for the target proteins.

211　　Expression experiments were then scaled up for protein purification.

212　　Starter cultures (10 mL M9ZB medium, containing kanamycin and chloramphenicol, both at

213　　50 µg/mL) were inoculated from glycerol stocks and grown overnight at 37 °C with 225 rpm

214　　orbital shaking. Dynamite medium (produced as described in Taylor *et al.* (2017) consisting

215　　of 12 g/L tryptone, 24 g/L yeast extract, 86 mM glycerol, 30 mM monopotassium phosphate,

216　　72 mM dipotassium phosphate, 1.6 mM magnesium sulphate, 28 mM glucose, with added

217　　kanamycin and chloramphenicol at 50 µg/mL) was seeded with the overnight starter culture

218　　(10 mL starter culture in 1 L Dynamite medium). This culture was grown for 3-4 h at 37 °C

219　　with shaking at 220 rpm until OD$_{595}$=0.6-0.8 and then IPTG (0.5 mM final concentration)

220　　added to initiate protein expression. Cultures were then transferred to 24 °C with 220 rpm

221　　shaking for 20 h. Cells were pelleted by centrifugation (5,000 × *g*, 4 °C, 20 min), washed with

222　　40 mL buffer (50 mM HEPES pH 7.2, 300 mM NaCl, 5 mM MgCl$_2$), transferred to 50 mL

223　　screw capped tubes before finally collecting by centrifugation (5,000 × *g*, 4 °C, 20 min). The

224　　pellet was flash frozen in liquid nitrogen and stored at -80 °C.

225　　Cell pellets were thawed on ice and resuspended in Lysis Buffer (50 mM HEPES pH 7.2, 5

226　　mM MgCl$_2$, 300 mM NaCl, 50 mM Imidazole, 0.1% Triton X-100 (v/v), 10 µM leupeptin, 1

227 mM PMSF), using 7 mL buffer for every 1 g of pellet. Cells were lysed on ice using a probe
228 sonicator and 5 cycles of 30 s on 30 s off until the solution was homogeneous. Cell debris
229 was removed by centrifugation (23,000 × *g*, 4 °C, 30 min) and the soluble fraction pushed
230 through a 0.45 µm syringe filter prior to chromatography.

231 Purification of the Rca protein was achieved using an NGC chromatography system (Bio-
232 Rad, UK), equipped with a nickel-charged IMAC column (1 mL HisTrap Fast Flow, Cytiva)
233 and a desalting column (10 mL Bio-Scale Mini Bio-Gel P6 Desalting Cartridge, Bio-Rad).
234 IMAC and desalting columns were equilibrated with Equilibration Buffer (5 mL: 50 mM
235 HEPES pH 8, 300 mM NaCl, 5 mM $MgCl_2$, 50 mM imidazole) and Final Buffer (13 mL: 50
236 mM HEPES pH 8, 5 mM NaCl, 5% glycerol), respectively. The sample was applied to the
237 IMAC column, followed by Wash Buffer (15 mL: 50 mM HEPES pH 8, 300 mM NaCl, 5 mM
238 $MgCl_2$, 125 mM imidazole). Bound protein was eluted using a higher concentration of
239 imidazole (2.1 mL: 50 mM HEPES pH 8, 300 mM NaCl, 5 mM $MgCl_2$, 300 mM imidazole)
240 and directly applied to the desalting column equilibrated in Final Buffer (50 mM HEPES pH
241 8, 5 mM $MgCl_2$, 5% glycerol). Fractions (1 mL) containing protein were identified using a
242 UV/Vis detector reading at 280 nm. Fractions containing the highest protein concentration
243 (determined using Bradford reagent, BIO-RAD) were pooled, ATP and DTT (0.2 mM and 5
244 mM final concentration respectively) added and 50-100 µL aliquots frozen in liquid nitrogen
245 before storage at -80 °C.

In vitro characterization of Rca thermal optima

247 The rate of ATP hydrolysis by Rca isoforms was assayed using the method described by
248 Chifflet *et al.* (1988), with modifications as described within Degen *et al.* (2020). ATP
249 hydrolysis was measured at a range of temperatures (20-55 °C, with 5 °C increments) using
250 5-minute assays, with reactions initiated through addition of Rca (final concentration 1 µM
251 Rca monomer) and quenched via addition of SDS. After quenching, all reactions and
252 standards were kept at 4 °C until inorganic phosphate (P_i) determination. The P_i released
253 during ATP hydrolysis was determined by measuring the absorbance of molybdenum blue at
254 850 nm in a spectrophotometer (SpectroStar Nano, BMG Labtech, UK).

255 Rubisco reactivation assays were conducted at a range of temperatures (20-45 °C, with 5 °C
256 increments) following the procedures of Barta *et al.* (2011) and Degen *et al.* (2020). Briefly,
257 Rubisco purified as per Amaral *et al.* (2024) was used to prepare inhibited Rubisco
258 complexes (ER) through spin-desalting purified Rubisco in CO_2 and Mg^{2+} free buffer followed
259 by incubation with RuBP overnight at 4 °C (as described in Barta *et al.*, 2011b). The two-
260 stage reactivation assay comprises a first stage assay where Rca is added to inhibited
261 Rubisco (ER) at a test temperature (20-45 °C, with 5 °C increments), with aliquots from this

262 assay taken at time intervals to initiate the second stage assay that measures Rubisco

263 activity. The Rubisco activity measured at each time-point is a function of the Rca, time

264 allowed for reactivation, and the temperature of the first stage (Supporting Information Fig.

265 S2). The first stage assays contained 5 mg/mL Rubisco, 1 mg/mL Rca and 5 mM ATP. With

266 known quantities of Rca and Rubisco, and appropriate controls, Rca reactivation of Rubisco

267 can be established following the calculations described within Degen *et al.* (2020). Maximum

268 Rubisco activity was determined at every temperature and was comparable among assays

269 with each of the four Rca isoforms.

270 Independent purifications of each isoform were used as biological replicates. For ATPase

271 activity, three biological replicates were measured for Rca8α and four for the each of the rest

272 of the isoforms. For Rubisco reactivation, four biological replicates were measured for

273 temperatures 20,25,30,32 °C and three for temperatures 38,40,45 °C. To estimate maximum

274 ATP hydrolysis and Rubisco activation activities and the corresponding temperatures at

275 which the maximum values are attained, second- to third-order polynomials and generalized

276 additive models (GAM) were fitted to the experimental data using the gam function from the

277 mgcv 1.8–24 package in R (Wood, 2017). The model that best fit the experimental data was

278 selected based on the Akaike information criterion using the AIC function (Akaike, 1974)

279 (Supporting Information Table S3). The selected model was fitted to each set of the

280 biological replicates (Table 1) as well as the whole dataset (Supporting Information Table

281 S4). T_{max} was calculated as the temperature corresponding to maximum activity. T_{opt} was

282 calculated as the range where activity was maintained above 70% of maximum value. $T_{0.5}$

283 was calculated as the temperature where activity dropped below 50% of maximum value.

Plant growth and sampling

285 *Vigna unguiculata* (L.) Walp. cv. IT97K-499-35 seeds (kindly provided by B.B. Singh) were

286 germinated in 0.6 L Deepots (D40H, Stuewe & Sons) containing 1:1 (v:v) mixture of nutrient-

287 rich compost (Petersfield Growing Mediums) and silver sand (horticultural grade, Royal

288 Horticultural Society). Plants were grown in eight growth cabinets (MC1000, Snijders Labs)

289 and watered as needed to soil saturation. Cabinets were maintained at day/night

290 temperatures of 28/18 °C, 70% relative humidity and 400 ppm CO_2 concentration (control

291 conditions). A 12 h photoperiod of constant light of 850 µmol m^{-2} s^{-1} at canopy level was

292 maintained via LED lighting (NS1 spectrum, Valoya). Four cabinets were randomly selected

293 to apply a heat treatment starting at 13 days after sowing (das) including an intermediate day

294 with day/night temperatures of 34/24 °C followed by 5 days of 38/28 °C (Supporting

295 Information Fig. S3a). Data loggers (OM-EL_USB-2, Omega Engineering Ltd.) were placed

296 at canopy level in each cabinet to record temperature and relative humidity every 15 minutes

297 (Supporting Information Fig. S3b).

298   Twenty cowpea plants were grown in each cabinet and sampled or measured for different

299   analyses following a randomised design (Supporting Information Fig. S4). All samples and

300   measurements were taken from the central leaflet of the first trifoliate leaf. Leaf disc samples

301   were taken 4-5 h into the light period, after which plants were cut above the unifoliate leaves

302   to reduce shading of neighbouring plants. Separate plants were used for sample collection in

303   subsequent time points. For non-destructive measurements, such as plant growth traits and

304   chlorophyll content, the same individuals were measured at all time points.

305   Growth measurements were obtained at 15, 17 and 22 das (days 2 and 4 of the heatwave

306   and on day 4 of the post-heatwave recovery period, Supporting Information Fig. S5). Leaf

307   chlorophyll content was estimated using a chlorophyll concentration meter (MC-100,

308   Apogee) by measuring 3 positions on the central leaflet for each plant. Plant height was

309   measured using a ruler from the soil level to the apical meristem. Leaf length and width

310   (widest part perpendicular to the length) were also measured with a ruler for the central

311   leaflet only. Leaf thickness was measured with a digitronic calliper 110-DBL (Moore &

312   Wright). Total above-ground biomass was determined on a separate set of plants by drying

313   leaves and stems at 60 °C until constant weight.

314   Chlorophyll fluorescence (method below) measurements were conducted every day of the

315   heatwave. Three 0.38 cm^2 leaf discs were excised and quickly placed with the adaxial

316   surface upwards on a single layer of wet filter paper on a thin plastic tray (<0.5 mm) and

317   immediately transported to the fluorescence imager.

318   A thermal imaging camera (CAT S60 smartphone, Caterpillar) was used prior to sampling to

319   assess T_{leaf}. Each image was later analysed with FLIR Thermal Studio software (Teledyne

320   FLIR LLC), providing the mean temperature across an area of the leaf surface (Supporting

321   Information Fig. S6).

322   For RNA-seq analyses (method below), four 0.55 cm^2 leaf discs were collected using a cork

323   borer from one leaf per plant. Four independent biological replicates (plants) were used per

324   treatment per timepoint (days 1, 3 and 5 of heatwave), and samples were immediately snap

325   frozen in liquid nitrogen and stored at -80 °C.

326   For protein and Rubisco analyses, four 0.55 cm^2 leaf discs were excised as above and

327   quickly placed with the adaxial surface upwards on a single layer of wet filter paper to

328   maintain turgidity. The filter paper was contained in a thin plastic tray and positioned on the

329   surface of the water in a circulating water bath in the artificial sunlight simulation rig (Taylor

330   *et al.*, 2022). PPFD at leaf-disc-level was $850 \text{ }\mu\text{mol m}^{-2}\text{ s}^{-1}$. Water bath temperature was

331   maintained at 26 °C or 32 °C (±0.1 °C) for control or heat-treated plants, respectively, to

332   mimic leaf temperatures in the growth cabinet. After 1 h incubation leaf discs were quickly

333   blotted on absorbent paper to remove excess moisture, then immediately frozen in liquid
334   nitrogen and stored at -80 °C.

335   For Rubisco reactivation in leaf extracts (LE), eight 0.55 cm^2 leaf discs were sampled on day
336   5 of the heatwave. A different plant was used for each of the seven temperatures of the
337   temperature response curve (20, 25, 32, 38, 40, 45 °C). Samples were quickly frozen in
338   liquid nitrogen, then stored at -80 °C until further analysis.

Chlorophyll fluorescence

340   Samples were analysed using a chlorophyll fluorescence imager (closed 800C FluorCam,
341   Photon System Instruments). The imager contained a customized temperature-controlled
342   sample surface area which comprised an aluminium plate with imbedded copper piping
343   connected to a circulating temperature-controlled water bath (Optima TX150, Grant
344   Instruments). The filter paper was in contact with sponges which acted as water reservoirs to
345   ensure the paper remained wet during analysis (Supporting Information Fig. S7a). The
346   temperature of the sample surface area and leaf discs were recorded using type k
347   thermocouples and a data logger (RDXL4SD, Omega). Additional thermocouple wires were
348   placed in contact with the sample surface area, and extra leaf discs, to record temperature
349   throughout the analysis (Supporting Information Fig. S7a). Samples were first dark adapted
350   for 1 h at 26 °C. After dark adaptation, the Fv/Fm protocol in the software (FluorCam 7,
351   Photon System Instruments) was used to make measurements of the maximum quantum
352   efficiency of photosystem II over a range of temperatures. The temperature of the leaf discs
353   was used to assess when the measurement temperature had been reached and was stable.
354   Once stable, the temperature was held for 3 min before the Fv/Fm measurement was
355   taken.

356   The data for each set of three leaf discs from the same plant were averaged and plateauing
357   Fv/Fm points at higher temperatures were removed before the remaining data were used to
358   calculate T$_{crit}$ (Supporting Information Fig. S7b) with the segmented function from the
359   segmented package(Muggeo, 2017) in R. This function uses a previously fitted linear model
360   to identify a breakpoint and fits two linear models before and after the breakpoint. The
361   breakpoint in the Fv/Fm curve was taken as T$_{crit}$ while the slopes of the two linear models
362   were taken as m1 & m2 (Supporting Information Fig. S7b, c, d).

Protein extraction, Rubisco activity and content

364   Proteins were extracted from leaf disc samples and Rubisco activity assays were performed
365   in a randomised order, as described previously (Taylor *et al.*, 2022; Ashton *et al.*, 2024). The
366   activation state of Rubisco was calculated as the ratio of initial to total activity. In short,

367   aliquots of the leaf extract supernatant were added to an assay mix containing $^{14}CO_2$ and

368   RuBP to initiate assays that gave an estimate of Rubisco initial activity, whereas Rubisco

369   total activity was measured after allowing a 3-minute incubation period of the leaf extract in

370   the assay mix without RuBP to allow full carbamylation of Rubisco.

371   Aliquots of leaf extract supernatant were also used for determining Rubisco content via ^{14}C-

372   CABP (2-carboxy-D-arabinitol 1,5-bisphosphate) binding, as previously described (Ruuska

373   *et al.*, 1998; Ashton *et al.*, 2024) and total soluble protein content, using the Bradford method

374   (Bradford, 1976).

Gene expressions analysis

376   Frozen leaf disc samples were ground to a fine powder in liquid nitrogen using a pestle and

377   mortar. Total RNA was extracted from 20-30 mg tissue using a NucleoSpin™ RNA Plant Kit

378   (Macherey-Nagel) including a DNase treatment, according to the manufacturer's

379   instructions. RNA concentration and quality were determined by spectrophotometry using a

380   microplate reader and LVis plate (SPECTROstar Nano, BMG Labtech) (Supporting

381   Information Table S5). Further QC analysis of RNA samples was performed by Novogene

382   using a Qubit fluorometer (Invitrogen) and an Agilent 5400 fragment analyzer, followed by

383   mRNA purification (using poly-T oligo-attached magnetic beads), library construction and 2 x

384   150 bp paired-end (PE150) sequencing using an Illumina NovaSeq 6000 (read depth of 30

385   million reads).

386   An initial filtering was applied to the raw data to remove reads containing adapters,

387   containing N > 10% (N represents bases that cannot be determined) and low-quality bases

388   (Phred < 5). Further read quality assessment and trimming was performed using the FastQC

389   tool, version 0.12.1 (http://www.bioinformatics.babraham.ac.uk/projects/fastqc/) and

390   cutadapt, version 4.2 (Martin, 2011). Low quality bases (Phred < 30) were trimmed from 3'

391   ends of each read, flanking N bases were removed and trimmed reads shorter than 50 bp

392   were discarded (for sequencing and alignment statistics see Supporting Information Table

393   S6).

394   Cowpea IT97K-499-35 reference transcriptome v1.2 (Lonardi *et al.*, 2019; Liang *et al.*, 2024)

395   was downloaded from Phytozome 13 (Goodstein *et al.*, 2012). Salmon, version 1.10.1 (Patro

396   *et al.*, 2017) was first used to index the reference transcriptome and then quantify expression

397   of clean reads at the transcript level. To identify changes in the cowpea Rca transcripts TPM

398   values were extracted from the Salmon Quant.sf output files for Rca, RbcS and HSP20

399   transcripts. Three transcripts are present for Rca1β (the first two result in the same protein,

400   the third is missing some of the N domain) and TPM values for all three were combined.

401   Three transcripts exist for Rca8α (transcripts 2 and 3 are non-functional and have low

402 expression) so here we only present data for the first transcript. For Rca10 transcripts 1, 3

403 and 4 are combined to give total expression for the alpha isoform and transcript 2 alone

404 represents the beta isoform. For RbcS, there are two genes on chromosomes 3 and 4, the

405 former only produces negligible transcript levels of expression while the latter produces high

406 levels of one transcript and low levels of two other transcripts – the three transcripts encoded

407 by the gene on chromosome 4 produce an identical protein and were combined.

408 Global gene expression analysis was carried out in R version 4.4.1 (2024-06-14, Race for

409 Your Life). Raw counts from Salmon were loaded into EdgeR 4.2.1 using tximport 1.32.0 and

410 rtracklayer 1.64.0. Transcript data for each gene was combined at this stage so that all

411 global analysis was performed at the gene-level. PCA plot was made using logCPM the

412 PCAtools 2.16.0 to check that biological replicates group together and to look for outlying

413 samples. Here we used the counts per million (CPM) to remove the variability due to library

414 depth. The EdgeR trimmed mean of M-values (TMM) method was used for normalisation of

415 read counts. The data was filtered using a CPM threshold to remove genes with zero or near

416 zero expression. A generalised linear model was then fitted to the normalised and filtered

417 data for each gene. Empirical Bayes quasi-likelihood F-tests were used to test whether

418 genes were significantly differentially expressed between heat-treated and control plants on

419 each day of the heatwave. To control for multiple testing, p-values were calculated using the

420 false discovery rate (FDR) of Benjamini-Hochberg. Differentially expressed genes (DEGs)

421 were then identified using the threshold values of a false discovery rate (FDR) of < 0.05 and

422 a log2 (|fold change|) of >1.5.

423 Rca gene expression changes were validated via RT-qPCR (Supporting Information Fig. S8)

424 to confirm transcript profiles of Rca isoforms. For sampling and detailed methodology see

425 Supporting Information Tables S7 & S8.

Rca quantification via western blotting

427 To quantify the abundance of different Rca protein isoforms, an aliquot of supernatant

428 resulting from Rubisco analysis was mixed with SDS-PAGE loading buffer and separated as

429 previously described on Perdomo *et al.* (2018) on a 12% TGX Stain-Free gel (Bio-Rad). Gels

430 were imaged to assess total protein before transfer to a nitrocellulose membrane using a dry

431 blotting system (iBlot2, Thermo Fisher Scientific). Membranes were stained with REVERT

432 Total Protein Stain for normalisation (Li-Cor Biosciences) and imaged prior to application of

433 antibodies. To compare the abundance of α and β isoforms of Rca, an antibody with broad

434 specificity for both isoforms was used (Feller *et al.*, 1998,a gift from Michael Salvucci), with

435 detection via a secondary fluor-tagged antibody (IRDye800CW, Li-Cor Biosciences,

436 RRID:AB_1660973). A dilution series of a pooled sample was run on every gel alongside the

437   samples to verify antibody detection was within the linear range. To quantify Rca8α, a more

438   specific antibody was used (Abcalis) in place of the broad specificity antibody. The anti-

439   Rca8α specific antibody was generated using phage display with the peptide selected

440   targeted against KRGAFYGKAAQQINVP (amino acid residue 376-391), as described in

441   Bloemers & Carmo-Silva (2024). All blot images were obtained using an Odyssey FC (Li-Cor

442   Biosciences). Empiria studio software (version 2.3.0.154, Li-Cor Biosciences) was used for

443   image data analysis and normalisation with the total protein stain, with values determined as

444   signal intensity.

Characterization of Rca thermal optima in leaf extracts

446   Rubisco reactivation by Rca in leaf extracts was determined as described in Carmo-Silva &

447   Salvucci (2011). Eight leaf discs per plant were sampled from the youngest fully expanded

448   leaf on day 5 of the heatwave. Separate samples were used for assaying each of the seven

449   temperatures of the temperature response curve shown in Figure 4, and eight plant sample

450   replicates were used per temperature. Samples were stored at -80 °C until further analysis.

451   One replicate of samples from one cabinet at control and one cabinet at high temperature

452   was used in each day of Rca assays, with samples allocated randomly to each assay

453   temperature. Supporting Information Fig. S9 illustrates the method which uses leaf extracts

454   as the source of both Rubisco and Rca, incubates sub-aliquots with different assays mixes,

455   and then carries out a two-stage assay very similar to the assay with the purified proteins.

456   This enables determination of the capacity of a population of Rca, drawn from plants grown

457   in different conditions, to reactivate Rubisco. Model fitting and temperature parameter (T_{max},

458   T_{opt} and $T_{0.5}$) calculations were conducted as described for the *in vitro* Rca activity assays

459   above and Rca activity was normalised on total soluble protein (TSP). Aliquots of the

460   desalted extract were used for total soluble protein (TSP) content determination using the

461   Bradford method (Bradford, 1976).

Data analyses

463   Geneious 2024.0.7 was used to generate protein alignments depicted in Figure 1a. Data

464   was processed using R 4.3.1 and RStudio 2024.09.0. Graphs were prepared using the

465   ggplot 2 (Wickham, 2017), EnhancedVolcano (Blighe *et al.*, 2018), VennDiagramm (Chen,

466   2022), ggpubr (Kassambara, 2023) and patchwork (Lin Pedersen, 2024) R packages.

467   Outliers were detected before statistical analysis with the Outliers package using Tukey's

468   fences method, where outliers are defined as extreme values that are 1.5 times the

469   interquartile range (1.5 IQR) below the first quartile or 1.5 IQR above the third quartile. Box

470   plots show medians and the first and third quartiles (25th and 75th percentiles), and whiskers

471   extend from the hinge to the largest or smallest value. Symbols represent individual data

472   points (technical or biological replicates defined for each plot either on methods or figure

473   legend). Bar plots show means and error bars represent standard error. For statistical

474   analysis, normality of data was assessed using the Shapiro-Wilk test and equality of

475   variances using the Levene test. For measurements on multiple days, two-way ANOVA tests

476   were applied to determine if there were significant day, treatment or interactive effects,

477   followed by post-hoc Tukey tests for multiple comparisons with Bonferroni

478   correction. Compact letters display (cld) were generated after the post-hoc pairwise

479   comparisons using packages mutlicomp (Bretz *et al.*, 2016) and multicompView (Graves *et*

480   *al.*, 2024). In cases where there was a slight violation of normality or homogeneity of

481   variance when data between different days was compared, two-way ANOVA was still

482   chosen as the most robust method. If normality and variance were severely violated, data

483   was log transformed, and two-way ANOVA was applied to the transformed data provided

484   assumptions were not severely violated in the transformed data. For the Rca isoform α/β

485   ratio, data was log transformed and analysis used the geometric mean. For measurements

486   taken at a single timepoint (growth parameters), t-test was used to determine statistical

487   significance between treatments. Statistical analysis results and full datasets are available

488   via Zenodo repository.

489   ## Results

490   ## Cowpea contains four Rubisco activase isoforms

491   The cowpea genome contains three genes that encode Rca. The gene on chromosome 1

492   (*Vigun01g219300)* encodes an Rca β, the gene on chromosome 8 (*Vigun08g150700)* an

493   Rca α, and the gene on chromosome 10 (*Vigun10g051600)* encodes both Rca α and β

494   isoforms via alternative splicing (Figure 1a). The gene on chromosome 8 also encodes a

495   truncated version of Rca, however this would not produce a canonical, fully functional Rca

496   as it has a premature stop codon before the α-helical domain which is necessary for the

497   recognition of Rubisco by Rca (Portis *et al.*, 2008). Rca isoforms in cowpea exhibit minor

498   sequence differences, primarily in the N-terminal region (the flexible domain critical for

499   Rubisco binding) (Stotz *et al.*, 2011; Shivhare *et al.*, 2019) and the α-helical domain

500   (Supporting Information Fig. S1).

501   ## Cowpea Rca isoforms differ in thermal optima of activity *in vitro*

502   Previous studies have shown the potential for intraspecies variation of Rca thermal optima

503   (Degen *et al.*, 2020). With four distinct isoforms in cowpea and its known ability to grow in

504   warm (20-37 °C) temperatures (Barros *et al.*, 2021), recombinant versions of each isoform

505   were produced for *in vitro* characterisation of cowpea Rca thermal optima (Figure 1b). Both

506   enzyme activities were assessed, i.e., the ability to reactivate inhibited cowpea Rubisco and

507   the ATPase activity that drives reactivation (Robinson & Portis, 1989). Rubisco reactivation

508   by Rca was calculated after accounting for the spontaneous reactivation of Rubisco,

509   expressed as a percentage of maximum Rubisco activity. The spontaneous reactivation of

510   Rubisco, although insignificant at lower temperatures, increases with temperature

511   (Supporting Information Fig. S2) as the Rubisco catalytic site becomes more flexible. For all

512   the Rca isoforms, the temperature corresponding to the peak of activity (T_{max}), the range of

513   temperatures at which activity was maintained above 70% of the maximum value (T_{opt}) and

514   the temperature at which activity drops below 50% of the maximum ($T_{0.5}$) were consistently

515   higher for ATPase activity than for Rubisco reactivation activity (Table 1). A higher sensitivity

516   of Rubisco reactivation compared to ATP hydrolysis has been previously reported and may

517   be due to the interaction with Rubisco being the key step impacted by elevated temperatures

518   in Rca (Degen *et al.*, 2020). It has also been shown that while ATP hydrolysis can be

519   catalysed by Rca oligomers consisting of three subunits, Rubisco reactivation requires

520   oligomers containing more than three subunits (Keown *et al.*, 2013; Hazra *et al.*, 2015).
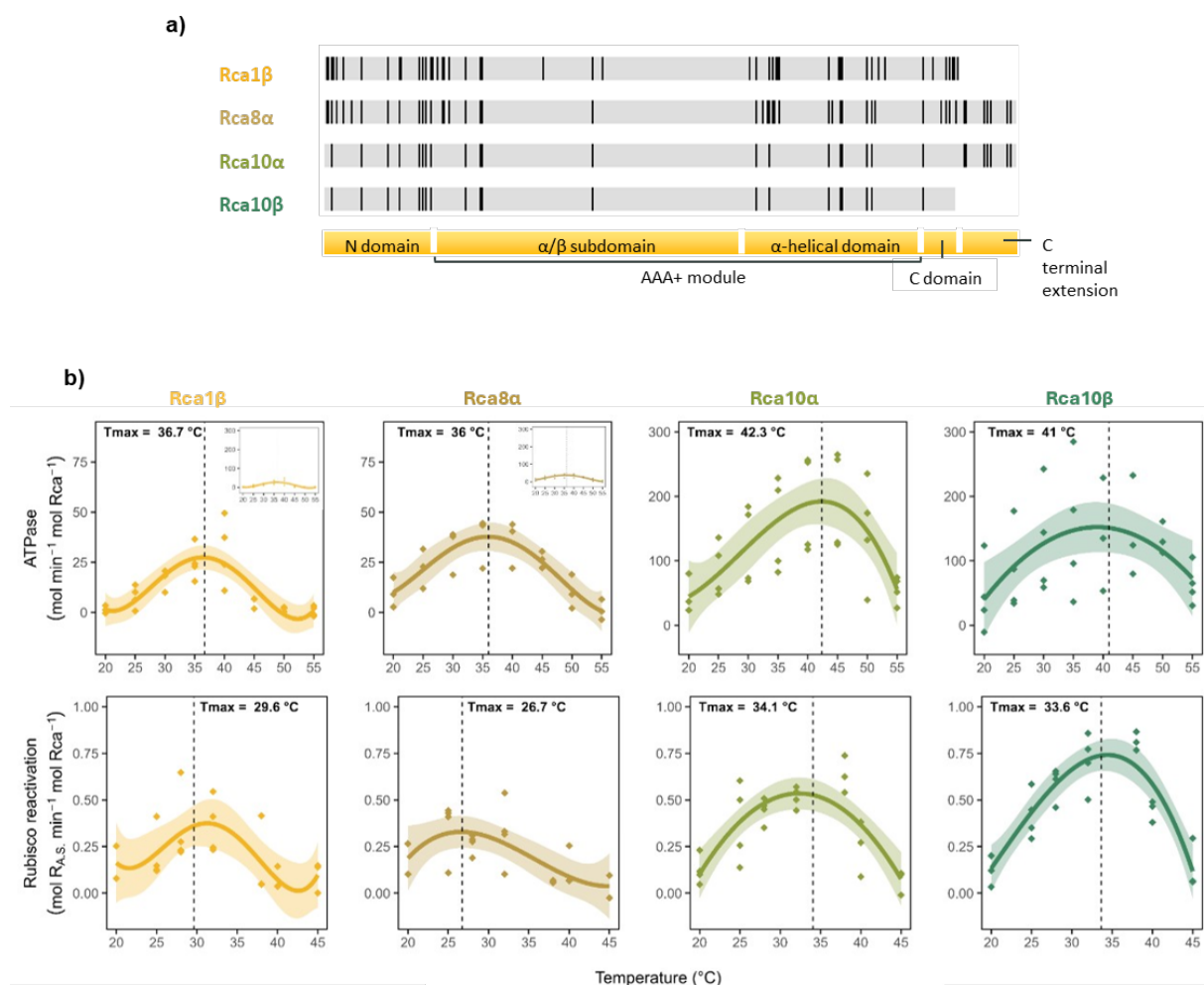
Figure 1. Temperature response of cowpea Rca isoforms in vitro. a) Amino acid residue alignment of the four cowpea Rca isoforms encoded by genes located on chromosomes 1, 8 and 10. Black vertical lines indicate differences in sequence among the genes. The following corresponding regions of the protein are shown: N-domain, α/β subdomain, α-helical domain, C-domain, and C-terminal extension. b) Temperature response of ATP hydrolysis and Rubisco activation by cowpea Rubisco activase isoforms *in vitro*. Rate of ATP hydrolysis and Rubisco reactivation by recombinantly produced purified cowpea Rca isoforms Rca1β, Rca8α, Rca10α and Rca10β. For Rca1β and Rca8α, subplots are included with the ATPase temperature response plotted with the y-axis on the same scale as the isoforms Rca10α and Rca10β. Dotted vertical line denotes T_{max}. Assays were performed at the indicated temperatures using 1 µM purified Rca and 5 mM ATP. Activation of pre-inhibited Rubisco used 5 µM Rubisco active sites ($R_{A.S.}$) in the ER form (1:5 Rca:$R_{A.S}$). Rubisco activation is presented relative to maximum Rubisco activity, determined as the Rubisco activity when Rca is allowed to reactivate inhibited Rubisco for 5 min. Values represent biological replicates (independent purifications; n=3-4 biological replicates). Lines represent the best fit

537   for each enzyme (selected by the Akaike information criterion) and shaded areas denote the

538   95% confidence interval for each fit (Supporting Information Table S3).

539   **Table 1.Temperature response of *in vitro* Rubisco activase (Rca) activity.** Maximum

540   rate of ATP hydrolysis and Rubisco activation and corresponding temperature (T_{max}),

541   optimum temperature range (T_{opt}, above 70% activity) and temperature above the optimum

542   at which 50% of the maximum activity remains ($T_{0.5}$). Values were estimated from best-fit

543   models that describe the *in vitro* temperature response of each Rca isoform (Supporting

544   Information Table S3). The best-fit model was applied to each of three biological replicates

545   with complete temperature response curves shown in Figure 1b. The first biological replicate

546   was excluded from the fitting of the individual replicates because the temperature response

547   of Rca activity was incomplete (determined only up to 32°C); this replicate is included in the

548   model fitting to the complete temperature response data set (Supporting Information Table

549   S4). Values show here are the mean ± standard error of the mean of values determined for

550   individual replicates of temperature response curves (n=3).

Rca Isoform	$ATPase_{max}$ (mol min^{-1} mol Rca^{-1})	T_{max} (°C)	T_{opt} (°C)	$T_{0.5}$ (°C)
1β	27.9 ± 5.5	36.7 ± 0.5	29.8 – 43.3	45.6 ± 1.1
8α	35.4 ± 5.5	36.0 ± 0.8	25.9 – 46.1	49.1 ± 0.5
10α	193.8 ± 39.3	42.3 ± 1.0	31.7 – 50.8	53.0 ± 0.6
10β	185.5 ± 58.2	41.0 ± 1.2	29.8 – 52.1	53.5 ± 0.3
Rca Isoform	Rubisco reactivation$_{max}$ (mol R$_{A.S.}$ min^{-1} mol Rca^{-1})	T_{max} (°C)	T_{opt} (°C)	$T_{0.5}$ (°C)
1β	0.38 ± 0.12	29.6 ± 0.8	25.6 – 34.6	36.7 ± 0.9
8α	0.39 ± 0.07	26.7 ± 0.9	23.4 – 31.5	33.7 ± 0.0
10α	0.54 ± 0.02	34.1 ± 0.8	26.4 – 40.6	42.4 ± 0.2
10β	0.82 ± 0.07	33.6 ± 0.2	26.6 – 40.1	42.0 ± 1.1

551

552   The two Rca isoforms encoded by *Rca10* were faster at hydrolysing ATP and reactivating

553   Rubisco, had higher thermal maxima (T_{max}), broader thermal optima (T_{opt}), and showed

554   thermal sensitivity ($T_{0.5}$) at warmer temperatures compared to the other two isoforms (Figure

555   1b;Table 1). T_{max}, T_{opt}, and $T_{0.5}$ calculated for both ATP hydrolysis and Rubisco reactivation

556   were generally similar for Rca1β and Rca 8α (Table 1), but Rca8α exhibited the lowest $T_{0.5}$

557   for reactivation activity (33.7 ± 0 °C). Up to 33.5 °C, all Rca isoforms maintained at least

558   70% of maximum Rubisco reactivation activity. Rca10α exhibited the highest temperature

559   corresponding to the peak of activity *in vitro* for both ATP hydrolysis (T_{max} = 42.3 ± 1 °C) and

560   Rubisco reactivation (T_{max} = 34.1 ± 0.8 °C). *In vitro* T_{max} values for Rca10α and Rca10β were

561   at least 3 °C higher for both ATP hydrolysis and Rubisco reactivation relative to Rca1β and

562   Rca8α (Table 1). Combined, the results show that the cowpea Rca10α and Rca10β isoforms

563   have faster rates, higher thermal maxima, broader thermal optima, and are less sensitive to

564   warmer temperatures than Rca1β and Rca8α.

A 5-day heatwave of +10 °C causes mild heat stress in cowpea

566   To investigate heat-induced changes in cowpea Rca *in planta*, young plants were exposed

567   to a 5-day heatwave consisting of an increase of 10 °C during both day and night. Plants

568   were cultivated for two weeks at 28/18 °C day/night, then in half of the controlled

569   environment cabinets the temperature was increased to 34/24 °C day/night for one day and

570   subsequently to 38/28 °C day/night for five days (Figure 2a, Supporting Information Fig. S3,

571   S4). The intermediate day aimed to resemble a gradual increase in temperature in field

572   conditions. Plants were well watered throughout the heatwave as the focus was on the

573   impact of heat on Rca and we wanted to avoid confounding effects of water deficit on CO_2

574   diffusion and assimilation. Cabinet and leaf temperatures were monitored throughout the

575   experiment to ensure the plants were under heat stress conditions, with heat-treated plants

576   showing a 6 °C increase in leaf temperature to 32 °C (Figure 2a, Supporting Information Fig.

577   S6). Thus, plants experiencing the heatwave had leaf temperatures within the T_{opt} of Rca

578   activity.

579   Plant growth traits were determined four days after the heatwave (day 22 of growth), after

580   plants were allowed to recover, and showed that the 5-day heatwave of +10 °C had only a

581   mild impact on cowpea (Figure 2b). Exposure to elevated temperature resulted in decreased

582   leaf thickness and increased plant height; however, no effect on aboveground dry biomass

583   was observed. Total chlorophyll also decreased in leaves that had been exposed to heat

584   when determined four days after the heatwave (Figure 2b). Measurement of leaf and plant

585   traits during the heatwave suggested an initial increase in the rate of cowpea leaf and plant

586   growth (day 2, Supporting Information Fig. S5), but only minimal differences between control

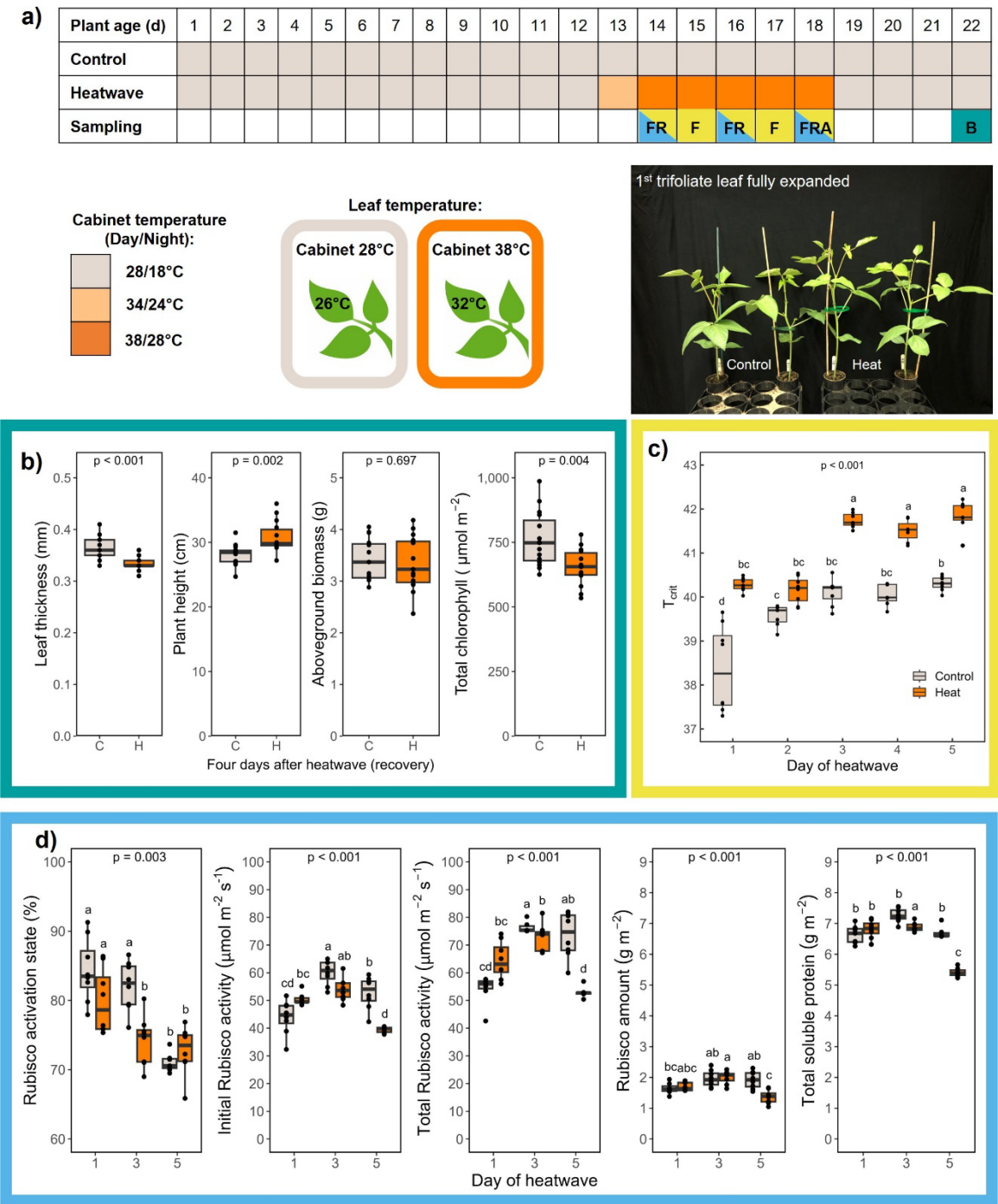587   and heat at the end of and after the heatwave.

Figure 2. Cowpea response to a heatwave in controlled environment. a) Experimental design, heatwave and sampling times. Plants were grown at 28/18 °C day/night for 13 days, then exposed to an intermediate heat treatment for a day at 34/24 °C day/night before being exposed to a 38/28 °C day/night heatwave for five days. Sampling: (F) photosystem II maximum efficiency (Fv/Fm) was measured daily during the heatwave; (R) leaf discs for RNA-seq analysis, total soluble protein (TSP), Rubisco activity and amount were sampled on days 1, 3 and 5 of the heatwave; (A) samples for Rca temperature response in leaf extracts were taken on day 5 of heatwave; (B) growth parameters and biomass were measured on

597   day 22 of plant growth, four days after the end of the heatwave (recovery). Cabinet and leaf

598   temperature were monitored daily. b) Leaf and whole plant growth parameters were

599   measured four days after the end of the heatwave (n=15). Relative chlorophyll content was

600   determined using a concentration meter based on leaf reflectance. c) T_{crit} was calculated for

601   each day of the heatwave as the breaking point where the two Fv/Fm slopes meet

602   (Supporting Information Fig. S7). d) Rubisco activation state (n=7-8), (b) initial (n=7-8) and

603   (c) total activity per leaf area (n=6-8), Rubisco amount (n=7-8) and total soluble protein

604   (TSP; n=6-8) were measured in leaf extracts on days 1, 3 and 5 of the heatwave. P-values

605   were calculated using two-way ANOVA followed by Tukey post-hoc tests.

606

607   As a proxy for photosynthetic activity, photosystem II (PSII) maximum efficiency (Fv/Fm) was

608   monitored throughout the heatwave (Supporting Information Fig. S7). Changes in Fv/Fm

609   indicate modifications in the functionality of PSII reaction centres, with a decrease indicating

610   photooxidative damage and reduced photochemistry quantum yield (Murchie & Lawson,

611   2013). Fv/Fm data collected from plants throughout the heatwave enabled determination of

612   T_{crit} (Figure 2c), which corresponds to the temperature at which chlorophyll *a* fluorescence

613   rises rapidly in response to temperature due to thermal damage in PSII, and is used as an

614   indicator of photosynthetic thermal stability (Perez & Feeley, 2020; Posch *et al.*, 2022). T_{crit}

615   slightly increased in control plants from day 1 to day 3 of the experiment as the leaf

616   developed (Figure 2c). In heat-treated cowpea, Fv/Fm did not decline compared to control

617   plants (Supporting Information Fig. S7e), indicating that no irreversible damage was caused

618   to PSII reaction centres due to heat stress. In fact, heat-treated plants showed a progressive

619   increase in the temperature at which Fv/Fm decreased, resulting in a significantly higher T_{crit}

620   after 3 days, denoting increased PSII thermal stability (p < 0.001, Figure 2c). These results

621   indicate a dynamic response that allows for PSII efficiency to adapt to warmer conditions.

Heat stress induces a decline in Rubisco activation state

623   In contrast to T_{crit}, the activation state of Rubisco decreased during the heat treatment

624   (Figure 2d). Importantly, a decline in Rubisco activation was observed from the beginning to

625   the end of the experiment as leaves aged. This decline was observed earlier in heat-treated

626   plants (day 3) compared to control plants (day 5), indicating that heat stress accelerated this

627   decline in Rubisco function. Rubisco activation state, defined as the ratio of initial to total

628   Rubisco activity, reflects the enzyme's operational efficiency under different conditions. Initial

629   activity represents the enzyme's immediate functionality upon extraction, while total activity

630   reflects its potential after full carbamylation (Ashton *et al.*, 2024). Although Rubisco

631   activation state was similar on day 5, the initial and total activity was significantly lower in

632   heat-treated compared to control plants ($p < 0.001$, Figure 2d). This decrease in Rubisco

633   activity on day 5 of the heatwave was associated with decreased Rubisco amount and TSP

634   (Figure 2d), as no significant differences were detected in leaf thickness during the heatwave

635   nor in Rubisco specific activity, expressed per quantity of Rubisco protein (Supporting

636   Information Fig. S5 & S10).

Heat stress induces the expression of thermotolerant Rca isoforms

638   Potential heat-induced changes in gene expression of *Rca* isoforms were assessed through

639   RNA sequencing analysis (RNA-seq) on days 1, 3 and 5 of the heatwave. A principal

640   component analysis (PCA) distinguished gene expression changes caused by heat stress

641   and those resulting from leaf aging (Figure 3a, Supporting Information Fig. S11). Heat-

642   induced differential gene expression occurred from the first day of the heatwave, with both

643   up and down-regulation of genes evident in heat-treated plants compared to control

644   conditions throughout the duration of the heatwave (Supporting Information Fig. S11). Heat

645   stress was confirmed by upregulation of the heat shock protein *HSP20* (Song *et al.*, 2017)

646   from day 1 of the heatwave (Figure 3b). The heatwave also decreased expression of the

647   Rubisco small subunit (*RbcS*), which is likely associated with the lower Rubisco amounts

648   (Figure 3c).

649   Under control temperature conditions, *Rca1β* was found to be the most abundant Rca

650   transcript, followed by *Rca8α*, while *Rca10α* and *Rca10β* were expressed at much lower

651   levels (Figure 3c). Of the hundreds of up and downregulated genes (Supporting Information

652   Fig. S11), volcano plots showed that *HSP20* and *Rca10* were both upregulated on days 1, 3,

653   and 5 of the heatwave (Supporting Information Fig. S12). Heat-treated plants showed a

654   (non-significant) tendency for lower *Rca1β* expression, whereas *Rca8α*, *Rca10α* and

655   *Rca10β* were all upregulated during the heatwave (Figure 3c). It is noteworthy that despite

656   the upregulation of both *Rca10* transcripts, their expression levels remained much lower

657   than *Rca1β* and *Rca8α* (Figure 3c)*. Changes in *HSP20* and the four *Rca* transcript levels

658   were also confirmed via RT-qPCR (Supporting Information Fig. S8). Moreover, promoter

659   analysis revealed multiple stress responsive elements in *Rca1β and Rca8α*, while *Rca10*

660   contains two heat stress response elements and has fewer other stress responsive elements

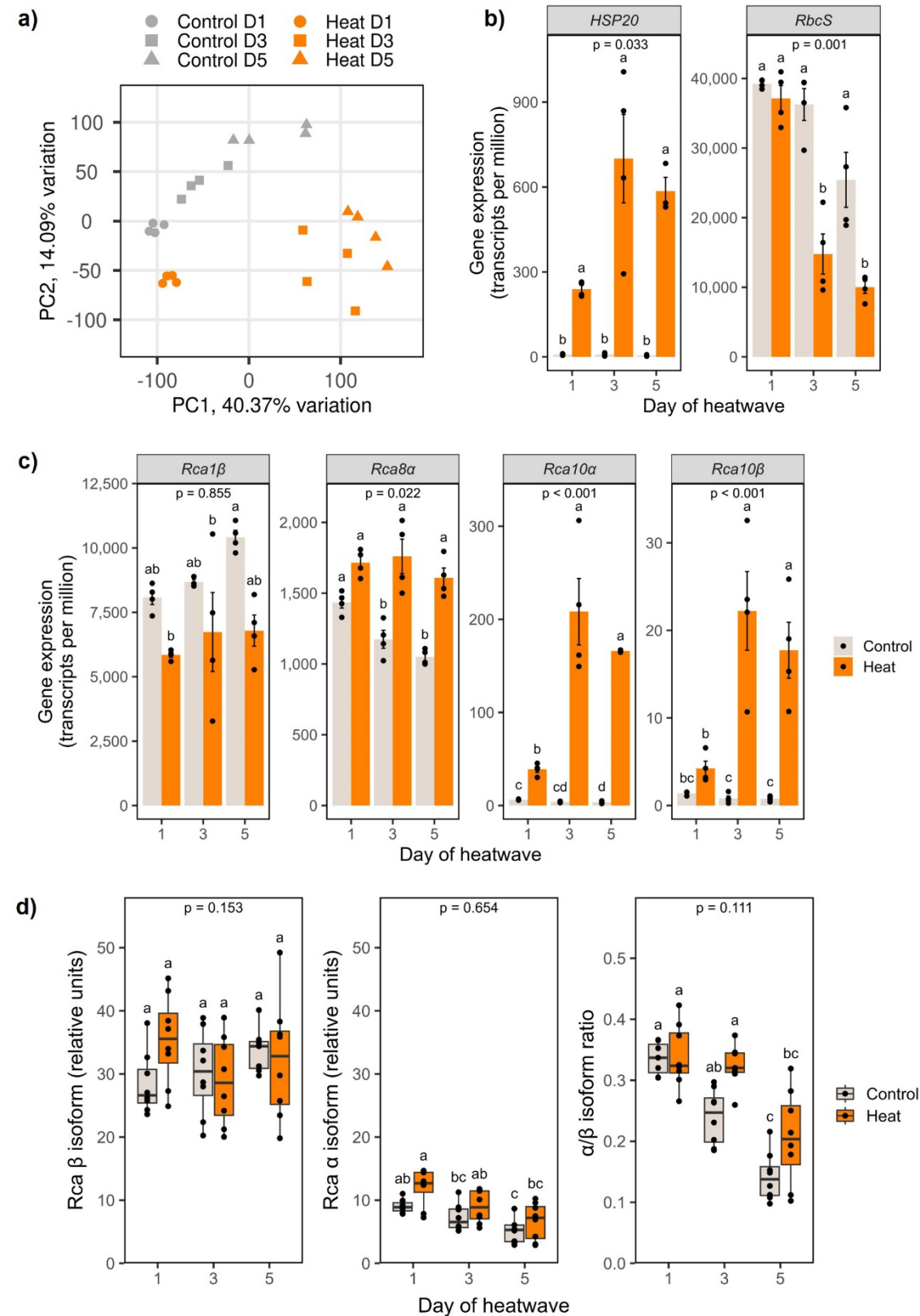661   (Supporting Information Fig. S13).

662

Figure 3. Differential gene expression and Rca protein abundance in cowpea during a heatwave. a) Principal components (PCA) plot of gene expression in leaves of heat-treated and control cowpea plants on days 1, 3 and 5 of the heatwave. b) Expression levels of the

666   heat shock protein 20 (HSP20) and the small Rubisco subunits (RbcS) were used as

667   reference. Bar plots represent means and error bars standard error. c) Expression levels of

668   the four cowpea Rca isoforms in control and heat-treated plant on days 1, 3 and 5 of the

669   heatwave (n=4). d) Protein abundance of Rca isoforms in leaves of control and heat-treated

670   plants on days 1, 3 and 5 of the heatwave (relative units). Rca α and β isoforms were

671   detected using an anti-Rca antibody and normalised to total protein. The size difference

672   between the α (45 kDa) and β (41 kDa) isoforms enabled the identification as separate

673   bands, and the estimation of the α/β ratio. P-values were calculated using two-way ANOVA

674   followed by Tukey post-hoc tests. For the α/β ratio, ANOVA was performed after log

675   transformation and using the geometric mean. Samples were run in separate gels and

676   normalised to total protein via reversible staining of the membrane.

677

678   To investigate if changes in gene expression are reflected at protein level, the abundance of

679   leaf Rca protein was quantified via immunoblotting (Figure 3d). A pan-Rca antibody that

680   reacts with all isoforms of Rca and enables quantification of Rca α and Rca β isoforms, as

681   these run separately in gel electrophoresis due to the difference in molecular weight, was

682   used to identify changes in abundance between α and β isoforms (Perdomo *et al.*, 2018).

683   Whilst differential gene expression was observed, changes in Rca protein were less

684   pronounced. As *Rca10β* transcript levels are almost negligible compared to *Rca1β*, it is

685   reasonable to infer that the β isoform protein is predominantly attributable to *Rca1β*

686   expression. Expression of *Rca8α* is also likely to produce most of the α isoform protein. Rca

687   β remained unchanged during the heatwave, while the α isoform decreased from day 1 to

688   day 5 but was not significantly different between control and heat-treated plants (Figure 3d).

689   Protein abundance of Rca8α was also determined using a specific antibody that only reacts

690   with this isoform (Bloemers & Carmo-Silva, 2024). Rca8α showed a near identical pattern to

691   the pan-Rca antibody for Rca α with a non-significant tendency for increased abundance in

692   heat treated plants compared to the control (Supporting Information Fig. S14a). The Rca

693   isoform α/β ratio was lower in day 5 compared to day 1 for both control and heat-treated

694   plants, and although no significant difference was found between treatments, a trend can be

695   seen for heat treated plants to maintain higher α/β ratio in days 3 and 5 (Figure 3d). Due to

696   their very low abundance, Rca10α & Rca10β protein isoforms were undetected in leaf

697   extracts with Rca10 specific antibodies (Supporting Information Fig. S14b).

Heat-treated plants maintain Rca rate and thermal optimum

699   To test the hypothesis that heat-induced changes in the relative abundance of Rca isoforms

700   are reflected in activity, we characterised the temperature response of Rubisco reactivation

701   by Rca in protein extracts from leaves sampled on day 5 of the heatwave (Figure 4). Leaf

702   extracts were desalted to produce the free Rubisco apoenzyme (uncarbamylated form),

703   which was subsequently inhibited through incubation with RuBP (Carmo-Silva & Salvucci,

704   2011). The inhibited Rubisco in the leaf extract was then used to determine the rate of

705   reactivation by the Rca holoenzyme via removal of RuBP from uncarbamylated Rubisco

706   catalytic sites, at a range of temperatures (Supporting Information Fig. S9). Concurrent

707   measurement of spontaneous reactivation of Rubisco in the absence of ATP, which is

708   required for Rca activity, enabled calculation of the spontaneous (Supporting Information

709   Fig. S15) and Rca-mediated rate of Rubisco reactivation (Figure 4).

710
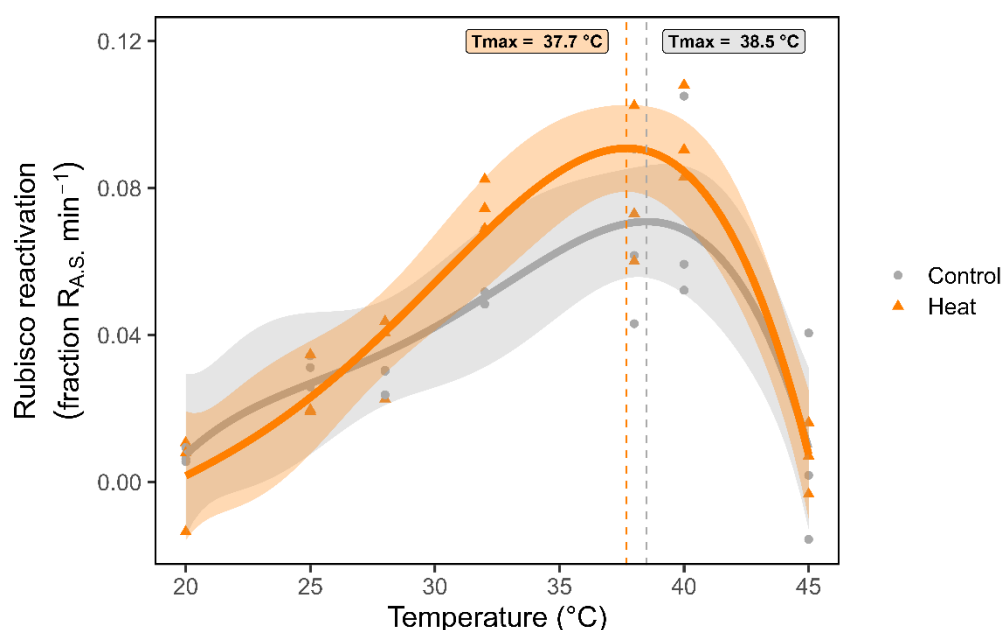
711   **Figure 4. Temperature response of Rca activity in leaf extracts of control and heat-**

712   **treated cowpea plants.** Leaf discs were sampled on day 5 of the heatwave. The Rubisco

713   and Rca contained in the leaves of each plant were extracted, Rubisco was inhibited by

714   binding of RuBP to decarbamylated catalytic sites in the absence of CO_2 and Mg^{2+}, then

715   reactivation by Rca was measured at varying temperatures by comparing an assay in

716   presence of ATP and ATP-regenerating system with the negative control assay in the

717   absence of ATP. The rate of Rubisco reactivation was calculated from measurements of

718   Rubisco activity at 30 and 90 s after the start of the assay and expressed relative to

719   maximum Rubisco activity in the same leaf extracts (as described in Supporting Information

720   Fig. S9). Symbols represent biological replicates (leaf extracts from independent plant

721   samples; n=8). Lines represent the best fit for each group of plants (selected by the Akaike

722   information criterion) and coloured areas denote the 95% confidence interval for each fit

723   (Supporting Information Table S9).

724

725   Rubisco reactivation by Rca tended to be faster in heat-treated compared to control plants,

726   however this increase was not statistically significant (*p = 0.339*, Figure 4). Heat-treated

727   plants exhibited similar thermal optima of Rubisco reactivation by Rca to control plants at

728   approximately 38 °C (Figure 4). T_{opt} and $T_{0.5}$ were also similar between control and heat-

729   treated plants (Table 2), indicating that the large fold-change in *Rca10* transcript abundance

730   (Figure 3c) and the small change in heat-induced protein Rca isoform ratio (Figure 3d) did

731   not alter the temperature profile of Rubisco reactivation by Rca in the leaves of heat-treated

732   plants (Figure 4). Interestingly, the T_{max}, T_{opt} and, to a lesser extent, $T_{0.5}$ of Rubisco

733   reactivation by Rca were higher in leaf extracts (Table 2) than the respective values

734   measured for each individual Rca isoform purified after recombinant expression (Table 1).

735

736   **Table 2. Temperature response of Rubisco activase (Rca) activity in leaf extracts.**

737   Maximum rate of Rubisco activation and corresponding temperature (T_{max}), optimum

738   temperature range (T_{opt}, above 70% activity) and temperature above the optimum at which

739   50% of the maximum activity remains ($T_{0.5}$). Values were estimated from best-fit models that

740   describe the temperature response of the pool of Rca isoforms extracted from leaves of control

741   and heat-treated cowpea on day 5 of the heatwave (Supporting Information Table S9). The

742   best-fit model for each treatment was applied to combined replicates shown in Figure 4 (n=6-

743   8).

Treatment	Rubisco reactivation$_{max}$ (fraction $R_{A.S.}$ min^{-1})	T_{max} (°C)	T_{opt} (°C)	$T_{0.5}$ (°C)
Control	0.07	38.5	31.9 – 42.6	43.4
Heat	0.09	37.7	31.4 – 42.2	43.3

744

Discussion

Cowpea Rca isoforms differ in thermal optima

We investigated the temperature response of Rubisco activase in cowpea, a vital crop for sub-Saharan Africa that is adapted to warm temperatures, yet susceptible to the increasing pressures of global warming. Several studies demonstrated that Rca thermolability limits photosynthesis at elevated temperatures (Feller *et al.*, 1998; Crafts-Brandner & Law, 2000; Salvucci *et al.*, 2006; Perdomo *et al.*, 2017), making it a target for enhancing crop yield under elevated temperatures. In this study, we identified and characterised four Rca isoforms in cowpea: Rca1β, Rca8α, Rca10α and Rca10β. The relatively minor amino acid differences between the four sequences may contribute to functional diversity of Rca in cowpea, potentially allowing for fine-tuning regulation of Rca in response to the environment. *In vitro* analysis across a range of temperatures revealed a higher thermal optimum for Rca10α and Rca10β for both ATPase and Rubisco reactivation activities (Figure 1b). The most abundant Rca1β and Rca8α isoforms in cowpea leaves (Figure 3) both exhibited lower thermal optima and thermal maxima, as well as slower rates of catalysis for both activities compared to the isoforms encoded by *Rca10* (Table 1).

Differences in thermal optima among isoforms have been reported for other species. In rice, the α isoform is more thermotolerant while in wheat one of the two β isoforms exhibits a higher thermal optima (Scafaro *et al.*, 2018; Shivhare *et al.*, 2019; Degen *et al.*, 2020). For spinach, the β isoform is more sensitive to heat stress, with Rca β homo-hexamers displaying a lower thermal midpoint compared to Rca α homo-hexamers or hetero-hexamers comprising both α and β isoforms (Keown & Pearce, 2014). Notably, for all Rca isoforms, the T_{max} for ATPase activity is higher than for Rubisco reactivation, potentially due to differential oligomeric requirements for each activity. The proposed mechanism for Rca-mediated Rubisco reactivation involves threading Rubisco through the AAA+ pore, akin to the method employed by AAA+ ATPases that adjust the conformation of misfolded proteins (Bhat *et al.*, 2017; Houry *et al.*, 2017; Waheeda *et al.*, 2023). This mechanism requires hexameric Rca for Rubisco reactivation, whilst ATP hydrolysis can occur with three Rca subunits forming an oligomer (Keown *et al.*, 2013; Hazra *et al.*, 2015).

The maximum rates of both ATP hydrolysis and Rubisco reactivation were higher for the Rca10 isoforms compared to Rca1β and Rca8α (Table 1). Similar differences among Rca isoforms were observed in rice and wheat but only for ATP hydrolysis, with the more thermostable Rca isoforms exhibiting lower Rubisco reactivation maxima compared to the less thermostable isoforms (Scafaro *et al.*, 2016, 2019a; Shivhare & Mueller-Cajar, 2017; Degen *et al.*, 2020). In cowpea, we show that the increased thermostability of Rca10

780   isoforms occurs without a penalty in Rubisco reactivation rate. The broader T_{opt} of Rca10α

781   and Rca10β spans and extends above the T_{opt} of Rca1β and Rca8α (Table 1). Thus,

782   Rca10α and Rca10β appear to be ideal candidates to maintain CO_2 assimilation by Rubisco

783   both at optimal and supra-optimal temperatures. Curiously, the promoter regions of both

784   Rca1β and Rca8α contain multiple stress responsive elements while Rca10α and Rca10β

785   have only two heat response elements (Supporting Information Fig. S13), suggesting an

786   engineering approach may be required to alter the Rca isoforms predominantly involved in

787   maintaining Rubisco activity *in planta.*

Cowpea responds dynamically to a 5-day 38/28 °C heatwave

789   A 5-day heatwave at the vegetative growth stage (10 °C increase to 38/28 °C day/night) is

790   considered moderate heat stress for most cowpea cultivars (Lonardi *et al.*, 2019; Barros *et*

791   *al.*, 2021). Plants were well-watered to avoid confounding effects of water deficit limiting the

792   diffusion of CO_2 to Rubisco sites (Carmo-Silva *et al.*, 2012). The leaf temperature only

793   increased to 32 °C (Figure 2a), plant growth parameters were only mildly impacted, and the

794   aboveground dry biomass remained unaffected (Figure 2bc). Notably, it has been shown that

795   a heatwave during the vegetative stage can have a delayed impact on cowpea yield

796   (Mohammed *et al.*, 2024), which would not necessarily be expressed as reduced biomass at

797   the end of the heatwave. T_{crit}, an indicator of thermal lability of PSII, was higher on day 5 of

798   the 38/28 °C heatwave (Figure 2c) suggesting some capacity for PSII thermal acclimation

799   (Perez & Feeley, 2020). In wheat, increased T_{crit} after exposure to elevated temperature in

800   field and controlled environment experiments correlated with a dynamic response of PSII to

801   heat stress (Posch *et al.*, 2022). On day 5 of the 38/28 °C heatwave, cowpea plants had

802   decreased Rubisco activities and amount, lower leaf thickness, total chlorophyll and TSP

803   (Figure 2b). Similar results were observed in heat-treated maize (Qu *et al.*, 2023), which

804   could have a delayed impact on biomass production.

Thermotolerant Rca isoforms increase but remain low under heat

806   At optimal temperatures, *Rca1β* was the isoform most abundantly expressed, with *Rca8α*

807   following, while *Rca10α* and *Rca10β* were only marginally expressed (Figure 3c). Under

808   heat stress, *Rca8α*, *Rca10α* and *Rca10β* expression was upregulated, however *Rca10*

809   transcript levels remained very low compared to *Rca1β* and *Rca8α*. The corresponding

810   protein abundance was only marginally higher for Rca8α and remained undetectable for

811   Rca10α and Rca10β (Supporting Information Fig. S14; Figure 3d). The Rca α/β ratio

812   decreased as the leaves aged, and heat-treated plants showed a trend to maintain higher

813   α/β ratio than control pants on days 3 and 5, although this difference was not statistically

814   significant (Figure 3d). Variation in Rca α/β ratio under optimal and supra-optimal

815   temperatures may reflect differences in thermostability and regulatory mechanisms (Zhang &

816   Portis, 1999; Wang *et al.*, 2010; Degen *et al.*, 2021). While Rca α is subject to redox

817   regulation via thioredoxin-f (Zhang & Portis, 1999; Shivhare *et al.*, 2019; Kim *et al.*, 2020)

818   and tends to be more sensitive to inhibition by ADP (Zhang & Portis, 1999; Scafaro *et al.*,

819   2019b; Amaral *et al.*, 2024a), variation also exists in the properties of Rca β isoforms

820   (Scafaro *et al.*, 2019a; Perdomo *et al.*, 2019).

821   Changes in relative abundance of Rca isoforms under heat stress are species-specific

822   (Yamori & von Caemmerer, 2009). In *Arabidopsis*, the two isoforms are comparable in

823   thermotolerance and both increase with heat maintaining a 1:1 ratio (Ristic *et al.*, 2009).

824   Conversely, in rice and wheat, Rca isoforms differ in temperature response and heat induces

825   upregulation of the thermotolerant variants (Scafaro *et al.*, 2018, 2019a; Degen *et al.*, 2021).

826   While the same was observed for cowpea in the present study, the protein abundance of the

827   thermostable Rca isoforms remained below detection levels in plants exposed to the 5-day

828   38/28 °C heatwave. Overexpression of thermostable Rca via genetic engineering led to

829   enhanced photosynthesis and yield (Kurek *et al.*, 2007). Increasing Rca thermostability, and

830   to a lesser extent upregulation of its quantity, have been shown to ameliorate the reduction

831   in Rubisco activation state caused by elevated temperatures (Kurek *et al.*, 2007; Scafaro *et*

832   *al.*, 2018, 2019a; Kim *et al.*, 2020). The results presented here suggest that increasing

833   Rca10α and Rca10β abundance in cowpea, while possible in longer or hotter heat

834   conditions, would likely require an engineering approach.

835   Rubisco reactivation by Rca in cowpea remains unaltered under heat

836   The temperature response of Rubisco reactivation in leaf extracts of plants exposed to the 5-

837   day 38/28 °C heatwave showed a similar pattern and comparable thermal optima to control

838   plants (Figure 4). Scafaro *et al.* (2019a) reported increases Rubisco reactivation rate and $T_{0.5}$

839   of Rca in leaf extracts from heat-treated wheat. In cowpea, the minor increase in rate was

840   statistically insignificant and T_{opt} and $T_{0.5}$ were comparable between control and heat-treated

841   plants, with a slight increase of the T_{opt} range in heat-treated plants (Table 2). These results

842   indicate that the heatwave in the absence of water deficit caused only mild heat stress,

843   allowing plants to respond by adjusting isoform ratios in the leaf while preserving the Rca

844   rate and temperature response.

845   Interestingly, the T_{opt} upper bound determined in leaf extracts was 42 °C for control and

846   heat-treated plants, much higher than the T_{leaf} in heat-treated plants (Table 2, Figure 2a).

847   The maximum Rca rate in leaf extracts (Table 2) was also higher than the Rubisco

848   reactivation rate of each isoform measured *in vitro* (Table 1). Similar results were observed

849   in rice and wheat but only for the more thermostable isoforms (Scafaro *et al.*, 2016, 2019a).

850   Higher Rca rate in leaf extracts may be attributed to several possible factors: differences in

851   structural conformation of recombinant Rca, post-translational modifications that regulate

852   Rca activity in the leaf and are absent in recombinant proteins, hetero-hexamers comprising

853   different isoforms *in planta* exhibiting higher thermal optima, or interaction of Rca with other

854   components in the chloroplast. Chen *et al.* (2010) reported dynamic and reversible binding of

855   rice Rca to the thylakoid membrane while it is active in remodelling the conformation of

856   inhibitor-bound Rubisco. Binding of Rca to the thylakoid membrane has also been reported

857   during heat stress although its binding to the chloroplast ribosomes was proposed to have a

858   protective role (Rokka *et al.*, 2001). Moreover, heat stress has been shown to induce

859   association of Rca with β-subunit of chaperonin-60 (cpn60β), a potential heat shock

860   molecular chaperone (Salvucci, 2008). Thus, while *in vitro* analyses are useful to compare

861   the properties of the individual isoforms, *in vivo* analyses as shown here for cowpea enable

862   assessment of the overall Rca response within the chloroplast stroma.

Conclusion

864   Cowpea is a vital source of protein for sub-Saharan Africa, and depite being warm-adapted,

865   it is threatened by future heatwaves, which are likely to increase in intensity, duration, and

866   frequency. Here, we identified two isoforms of Rca that have higher thermal maxima,

867   broader thermal optima, and faster rates of ATP hydrolysis and Rubisco reactivation than the

868   predominant Rca isoforms present in cowpea leaves. We showed that a 5-day 38/28 °C

869   heatwave in the absence of water deficit caused leaf temperature to increase to 32 °C. Since

870   this temperature is below the temperature at which Rca activity decreased below 70% of

871   maximum for each Rca isoform, the impact of such a heatwave on Rubisco function and

872   biomass production was only mild. However, cowpea plants growing in smallholder farmer

873   fields in sub-Saharan Africa are likely to experience water deficit alongside warmer

874   heatwaves (Almazroui *et al.*, 2020; Song *et al.*, 2023). This combination can impact the

875   ability of the plant to cool its leaves leading to higher leaf temperatures (Carmo-Silva *et al.*,

876   2012; Fahad *et al.*, 2017; Sato *et al.*, 2024). Increasing the abundance of the superior

877   Rca10α and Rca10β isoforms characterised here provides an exciting opportunity to

878   enhance the resilience of cowpea and other crops to future extreme climates.

885

886 Competing interests:

887 The authors declare no conflicts of interest.

888

889 Author contributions:

890 E.C.S conceived and supervised the research. A.G., R.P., I.R., D.J.O., E.C.S. designed

891 experiments. M.T.P. designed and executed the cloning strategy. D.B., P.D.G., D.W.

892 produced and purified recombinant proteins. D.W. and C.J.A. purified Rubisco. D.B. and

893 A.G. performed ATP hydrolysis measurements. A.G. performed Rubisco reactivation

894 measurements. R.P. and I.R. performed heatwave experiments. R.P. performed RNAseq,

895 RT-qPCR and plant growth measurements. R.P. and P.D.G. performed promoter analyses.

896 I.R. performed fluorescence measurements. A.G., R.P. and C.J.A. determined activity and

897 amount of Rubisco and Rubisco activase in leaf extracts. A.G., R.P., C.J.A. and I.R.

898 analysed the data. A.G. and E.C.S. wrote the manuscript with help from all authors.

899

900 Data availability:

901 Data presented are available in the accompanying supporting information and via Zenodo

902 (DOI: 10.5281/zenodo.15227677). The RNA-seq data reported in this article has been

903 deposited in DDBJ's Sequence Read Archive (DRA) and are accessible through DRR

904 BioProject accession number PRJDB19806. Processed RNA-seq data are submitted in the

905 DDBJ's Genomic Expression Archive (GEA) and are accessible through the Experiment

906 accession number (E-GEAD-889).

907

References

Akaike H. **1974**. A new look at the statistical model identification. *IEEE Transactions on Automatic Control* **19**: 716–723.

Almazroui M, Saeed F, Saeed S, Nazrul Islam M, Ismail M, Klutse NAB, Siddiqui MH. **2020**. Projected change in temperature and precipitation over Africa from CMIP6. *Earth Systems and Environment* **4**: 455–475.

Amaral J, Lobo AKM, Carmo-Silva E. **2024a**. Regulation of Rubisco activity in crops. *New Phytologist* **241**: 35–51.

Amaral J, Lobo AKM, Carmo-Silva E, Orr DJ. **2024b**. Purification of Rubisco from Leaves. In: Covshoff S, ed. Photosynthesis : Methods and Protocols. New York, NY: Springer US, 417–426.

Ara N, Nakkanong K, Lv W, Yang J, Hu Z, Zhang M. **2013**. Antioxidant enzymatic activities and gene expression associated with heat tolerance in the stems and roots of two Cucurbit species ('*Cucurbita maxima*' and '*Cucurbita moschata*') and their interspecific inbred line "*Maxchata*". *International Journal of Molecular Sciences* **14**: 24008.

Ashton CJ, Page R, Lobo AKM, Amaral J, Siqueira JA, Orr DJ, Carmo-Silva E. **2024**. Radiometric determination of Rubisco activation state and quantity in leaves. In: Methods in Enzymology. Academic Press.

Bagati S, Rai GK, Bhadwal D, Berwal MK. **2021**. Biotechnological approaches for the development of heat stress tolerance in crop plants. In: Abiotic Stress Tolerance Mechanisms in Plants. CRC Press.

Barros JRA, Guimarães MJM, Silva RM e, Rêgo MTC, de Melo NF, de Melo Chaves AR, Angelotti F. **2021**. Selection of cowpea cultivars for high temperature tolerance: physiological, biochemical and yield aspects. *Physiology and Molecular Biology of Plants* **27**: 29–38.

Barta C, Carmo-Silva AE, Salvucci ME. **2011a**. Purification of Rubisco activase from leaves or after expression in *Escherichia coli*. *Methods in Molecular Biology (Clifton, N.J.)* **684**: 363–374.

Barta C, Carmo-Silva AE, Salvucci ME. **2011b**. Rubisco activase activity assays. *Methods in Molecular Biology (Clifton, N.J.)* **684**: 375–382.

Becker R, Schüth C, Merz R, Khaliq T, Usman M, Beek T aus der, Kumar R, Schulz S. **2023**. Increased heat stress reduces future yields of three major crops in Pakistan's Punjab region despite intensification of irrigation. *Agricultural Water Management* **281**: 108243.

Bhat JY, Thieulin-Pardo G, Hartl FU, Wendler P, Mili Ci C G, Bracher A, Maxwell A, Ciniawsky S, Mueller-Cajar O, Engen JR, *et al.* 2017. Mechanism of enzyme repair by the AAA + chaperone Rubisco activase. *Molecular Cell* **67**: 744–756.

Blighe, K, S Rana, M Lewis. **2018**. EnhancedVolcano: Publication-ready volcano plots with enhanced colouring and labeling.

Bloemers D, Carmo-Silva E. **2024**. Antibody design for the quantification of photosynthetic proteins and their isoforms. In: Covshoff S, ed. Photosynthesis : Methods and Protocols. New York, NY: Springer US, 405–416.

953 **Bradford MM**. **1976**. A rapid and sensitive method for the quantitation of microgram quantities
954 of protein utilizing the principle of protein-dye binding. *Analytical Biochemistry* **72**: 248–254.

955 **Bretz F, Hothorn T, Westfall P**. **2016**. *Multiple Comparisons Using R*. CRC Press.

956 **Brown AV, Conners SI, Huang W, Wilkey AP, Grant D, Weeks NT, Cannon SB, Graham**
957 **MA, Nelson RT**. **2021**. A new decade and new data at SoyBase, the USDA-ARS soybean
958 genetics and genomics database. *Nucleic Acids Research* **49**: D1496–D1501.

959 **Carmo-Silva AE, Gore MA, Andrade-Sanchez P, French AN, Hunsaker DJ, Salvucci ME**.
960 **2012**. Decreased CO_2 availability and inactivation of Rubisco limit photosynthesis in cotton
961 plants under heat and drought stress in the field. *Environmental and Experimental Botany* **83**:
962 1–11.

963 **Carmo-Silva AE, Salvucci ME**. **2011**. The activity of Rubisco's molecular chaperone,
964 Rubisco activase, in leaf extracts. *Photosynthesis Research* **108**: 143–155.

965 **Carmo-Silva AE, Salvucci ME**. **2013**. The Regulatory Properties of Rubisco Activase Differ
966 among Species and Affect Photosynthetic Induction during Light Transitions 1. *Plant*
967 *Physiology Ò* **161**: 1645–1655.

968 **Carmo-Silva E, Scales JC, Madgwick PJ, Parry MAJ**. **2015**. Optimizing Rubisco and its
969 regulation for greater resource use efficiency. *Plant, Cell & Environment* **38**: 1817–1832.

970 **Chen H**. **2022**. VennDiagram: Generate High-Resolution Venn and Euler Plots.

971 **Chen J-H, Tang M, Jin X-Q, Li H, Chen L-S, Wang Q-L, Sun A-Z, Yi Y, Guo F-Q**. **2022**.
972 Regulation of Calvin–Benson cycle enzymes under high temperature stress. *aBIOTECH* **3**:
973 65.

974 **Chen J, Wang P, Mi H-L, Chen G-Y, Xu D-Q**. **2010**. Reversible association of ribulose-1, 5-
975 bisphosphate carboxylase/oxygenase activase with the thylakoid membrane depends upon
976 the ATP level and pH in rice without heat stress. *Journal of Experimental Botany* **61**: 2939–
977 2950.

978 **Chifflet S, Torriglia A, Chiesa R, Tolosa S**. **1988**. A method for the determination of inorganic
979 phosphate in the presence of labile organic phosphate and high concentrations of protein:
980 Application to lens ATPases. *Analytical Biochemistry* **168**: 1–4.

981 **Crafts-Brandner SJ, Law RD**. **2000**. Effect of heat stress on the inhibition and recovery of
982 the ribulose-1,5-bisphosphate carboxylase/oxygenase activation state. *Planta* **212**: 67–74.

983 **Crafts-Brandner SJ, Salvucci ME**. **2000**. Rubisco activase constrains the photosynthetic
984 potential of leaves at high temperature and CO_2. *Proceedings of the National Academy of*
985 *Sciences of the United States of America* **97**: 13430–13435.

986 **Degen GE, Orr DJ, Carmo-Silva E**. **2021**. Heat-induced changes in the abundance of wheat
987 Rubisco activase isoforms. *New Phytologist* **229**: 1298–1311.

988 **Degen GE, Worrall D, Carmo-Silva E**. **2020**. An isoleucine residue acts as a thermal and
989 regulatory switch in wheat Rubisco activase. *Plant Journal* **103**: 742–751.

990 **Fahad S, Bajwa AA, Nazir U, Anjum SA, Farooq A, Zohaib A, Sadia S, Nasim W, Adkins**
991 **S, Saud S, *et al.*** **2017**. Crop production under drought and heat stress: Plant responses and
992 management options. *Frontiers in Plant Science* **8**.

993 **Feller U, Crafts-Brandner SJ, Salvucci ME**. **1998**. Moderately high temperatures inhibit
994 ribulose-1,5-bisphosphate carboxylase/oxygenase (Rubisco) activase-mediated activation of
995 Rubisco. *Plant Physiol* **116**: 539–546.

996 **Galmés J, Hermida-Carrera C, Laanisto L, Niinemets Ü**. **2016**. A compendium of
997 temperature responses of Rubisco kinetic traits: variability among and within photosynthetic
998 groups and impacts on photosynthesis modeling. *Journal of Experimental Botany* **67**: 5067–
999 5091.

1000 **Gonçalves A, Goufo P, Barros A, Domínguez-Perles R, Trindade H, Rosa EAS, Ferreira
1001 L, Rodrigues M**. **2016**. Cowpea (*Vigna unguiculata* L. Walp), a renewed multipurpose crop
1002 for a more sustainable agri-food system: nutritional advantages and constraints. *Journal of the
1003 Science of Food and Agriculture* **96**: 2941–2951.

1004 **Goodstein DM, Shu S, Howson R, Neupane R, Hayes RD, Fazo J, Mitros T, Dirks W,
1005 Hellsten U, Putnam N, *et al.*** **2012**. Phytozome: a comparative platform for green plant
1006 genomics. *Nucleic Acids Research* **40**: D1178–D1186.

1007 **Graves S, Piepho H-P, Selzer L, Dorai-Raj S**. **2024**. multcompView: Visualizations of Paired
1008 Comparisons.

1009 **Harboure P**. **2024**. WMO Global Annual to Decadal Climate Update.

1010 **Hatfield JL, Prueger JH**. **2011**. Agroecology: Implications for Plant Response to Climate
1011 Change. In: Crop Adaptation to Climate Change. Wiley-Blackwell.

1012 **Hazra S, Henderson JN, Liles K, Hilton MT, Wachter RM**. **2015**. Regulation of ribulose-1,5-
1013 bisphosphate carboxylase/oxygenase (Rubisco) activase. *The Journal of Biological Chemistry*
1014 **290**: 24222–24236.

1015 **Hermida-Carrera C, Kapralov MV, Galmés J**. **2016**. Rubisco catalytic properties and
1016 temperature response in crops. *Plant Physiology* **171**: 2549.

1017 **Houry WA, Wachter R, Prahlad V, Hayer-Hartl M, Bhat JY, Thieulin-Pardo G, Hartl FU**.
1018 **2017**. Rubisco activases: AAA+ chaperones adapted to enzyme repair. *Frontiers in Molecular
1019 Biosciences* **4**: 20.

1020 **Kassambara A**. **2023**. ggpubr: 'ggplot2' Based Publication Ready Plots.

1021 **Keown JR, Griffin MDW, Mertens HDT, Pearce FG**. **2013**. Small oligomers of ribulose-
1022 bisphosphate carboxylase/oxygenase (Rubisco) activase are required for biological activity.
1023 *The Journal of Biological Chemistry* **288**: 20607–20615.

1024 **Keown JR, Pearce FG**. **2014**. Characterization of spinach ribulose-1,5-bisphosphate
1025 carboxylase/ oxygenase activase isoforms reveals hexameric assemblies with increased
1026 thermal stability. *Biochem. J* **464**: 413–423.

1027 **Kilian J, Whitehead D, Horak J, Wanke D, Weinl S, Batistic O, D'Angelo C, Bornberg-
1028 Bauer E, Kudla J, Harter K**. **2007**. The AtGenExpress global stress expression data set:
1029 protocols, evaluation and model data analysis of UV-B light, drought and cold stress
1030 responses. *The Plant Journal* **50**: 347–363.

1031 **Kim SY, Stessman DJ, Wright DA, Spalding MH, Huber SC, Ort DR**. **2020**. *Arabidopsis*
1032 plants expressing only the redox-regulated Rca-α isoform have constrained photosynthesis
1033 and plant growth. *Plant Journal* **103**: 2250–2262.

1034 **Kumar A, Li C, Portis AR**. **2009**. *Arabidopsis thaliana* expressing a thermostable chimeric
1035 Rubisco activase exhibits enhanced growth and higher rates of photosynthesis at moderately
1036 high temperatures. *Photosynthesis Research* **100**: 143–153.

1037 **Kurek I, Chang TK, Bertain SM, Madrigal A, Liu L, Lassner MW, Zhu G**. **2007**. Enhanced
1038 thermostability of *Arabidopsis* Rubisco activase improves photosynthesis and growth rates
1039 under moderate heat stress. *The Plant Cell* **19**: 3230–3241.

1040 **Law RD, Crafts-Brandner SJ**. **2001**. High temperature stress increases the expression of
1041 wheat leaf ribulose-1,5-bisphosphate carboxylase/oxygenase activase protein. *Archives of*
1042 *Biochemistry and Biophysics* **386**: 261–267.

1043 **Li G, Mao H, Ruan X, Xu Q, Gong Y, Zhang X, Zhao N**. **2002**. Association of heat-induced
1044 conformational change with activity loss of Rubisco. *Biochemical and Biophysical Research*
1045 *Communications* **290**: 1128–1132.

1046 **Liang Q, Muñoz-Amatriaín M, Shu S, Lo S, Wu X, Carlson JW, Davidson P, Goodstein**
1047 **DM, Phillips J, Janis NM, *et al*. 2024**. A view of the pan-genome of domesticated cowpea
1048 (*Vigna unguiculata* [L.] Walp.). *The Plant Genome* **17**: e20319.

1049 **Lin Pedersen T**. **2024**. patchwork: The Composer of Plots.

1050 **Lonardi S, Muñoz-Amatriaín M, Liang Q, Shu S, Wanamaker SI, Lo S, Tanskanen J,**
1051 **Schulman AH, Zhu T, Luo M-C, *et al*. 2019**. The genome of cowpea (*Vigna unguiculata* [L.]
1052 Walp.). *The Plant Journal* **98**: 767–782.

1053 **Martin M**. **2011**. Cutadapt removes adapter sequences from high-throughput sequencing
1054 reads. *EMBnet.journal* **17**: 10.

1055 **Mathur S, Agrawal D, Jajoo A**. **2014**. Photosynthesis: Response to high temperature stress.
1056 *Journal of Photochemistry and Photobiology B: Biology* **137**: 116–126.

1057 **Mohammed SB, Ongom PO, Togola A, Boukar O**. **2024**. Enhancing Cowpea tolerance to
1058 elevated temperature: Achievements, challenges and future directions. *Agronomy* **14**: 513.

1059 **Moore CE, Meacham-Hensold K, Lemonnier P, Slattery RA, Benjamin C, Bernacchi CJ,**
1060 **Lawson T, Cavanagh AP**. **2021**. The effect of increasing temperature on crop photosynthesis:
1061 from enzymes to ecosystems. *Journal of Experimental Botany* **72**: 2822–2844.

1062 **Muggeo VMR**. **2017**. Interval estimation for the breakpoint in segmented regression: a
1063 smoothed score-based approach. *Australian & New Zealand Journal of Statistics* **59**: 311–
1064 322.

1065 **Murchie EH, Lawson T**. **2013**. Chlorophyll fluorescence analysis: a guide to good practice
1066 and understanding some new applications. *Journal of Experimental Botany* **64**: 3983–3998.

1067 **Nagarajan R, Gill KS**. **2018**. Evolution of Rubisco activase gene in plants. *Plant Molecular*
1068 *Biology* **96**: 69–87.

1069 **Orr DJ, Robijns AKJ, Baker CR, Niyogi KK, Carmo-Silva E**. **2023**. Dynamics of Rubisco
1070 regulation by sugar phosphate derivatives and their phosphatases. *Journal of Experimental*
1071 *Botany* **74**: 581–590.

1072 **Patro R, Duggal G, Love MI, Irizarry RA, Kingsford C**. **2017**. Salmon provides fast and bias-
1073 aware quantification of transcript expression. *Nature Methods* **14**: 417–419.

1074 **Perdomo JA, Buchner P, Carmo-Silva E**. **2021**. The relative abundance of wheat Rubisco
1075 activase isoforms is post-transcriptionally regulated. *Photosynthesis Research* **148**: 47–56.

1076 **Perdomo JA, Capó-Bauçà S, Carmo-Silva E, Galmés J**. **2017**. Rubisco and Rubisco
1077 activase play an important role in the biochemical limitations of photosynthesis in rice, wheat,
1078 and maize under high temperature and water deficit. *Frontiers in Plant Science* **8**: 490.

1079 **Perdomo JA, Degen GE, Worrall D, Carmo-Silva E**. **2019**. Rubisco activation by wheat
1080 Rubisco activase isoform 2β is insensitive to inhibition by ADP. *Biochemical Journal* **476**:
1081 2595–2606.

1082 **Perdomo JA, Sales CRG, Carmo-Silva E**. **2018**. Quantification of photosynthetic enzymes
1083 in leaf extracts by immunoblotting. *Methods in Molecular Biology (Clifton, N.J.)* **1770**: 215–
1084 227.

1085 **Perez TM, Feeley KJ**. **2020**. Photosynthetic heat tolerances and extreme leaf temperatures.
1086 *Functional Ecology* **34**: 2236–2245.

1087 **Portis AR**. **2003**. Rubisco activase - Rubisco's catalytic chaperone. *Photosynthesis Research*
1088 **75**: 11–27.

1089 **Portis AR, Li C, Wang D, Salvucci ME**. **2008**. Regulation of Rubisco activase and its
1090 interaction with Rubisco. *Journal of Experimental Botany* **59**: 1597–1604.

1091 **Posch BC, Hammer J, Atkin OK, Bramley H, Ruan Y-L, Trethowan R, Coast O**. **2022**.
1092 Wheat photosystem II heat tolerance responds dynamically to short- and long-term warming.
1093 *Journal of Experimental Botany* **73**: 3268–3282.

1094 **Qu L, Gu X, Li J, Guo J, Lu D**. **2023**. Leaf photosynthetic characteristics of waxy maize in
1095 response to different degrees of heat stress during grain filling. *BMC Plant Biology* **23**: 469.

1096 **Ristic Z, Momčilović I, Bukovnik U, Prasad PVV, Fu J, DeRidder BP, Elthon TE,
1097 Mladenov N**. **2009**. Rubisco activase and wheat productivity under heat-stress conditions.
1098 *Journal of Experimental Botany* **60**: 4003–4014.

1099 **Robinson SP, Portis AR**. **1989**. Adenosine triphosphate hydrolysis by purified Rubisco
1100 activase. *Archives of Biochemistry and Biophysics* **268**: 93–99.

1101 **Rokka A, Zhang L, Aro EM**. **2001**. Rubisco activase: An enzyme with a temperature-
1102 dependent dual function? *Plant Journal* **25**: 463–471.

1103 **Ruuska S, Andrews TJ, Badger MR, Hudson GS, Laisk A, Price GD, Caemmerer S von**.
1104 **1998**. The interplay between limiting processes in C3 photosynthesis studied by rapid-
1105 response gas exchange using transgenic tobacco impaired in photosynthesis. *Functional
1106 Plant Biology* **25**: 859–870.

1107 **Salvucci ME**. **2008**. Association of Rubisco activase with chaperonin-60b: a possible
1108 mechanism for protecting photosynthesis during heat stress. *Journal of Experimental Botany*
1109 **59**: 1923–1933.

1110 **Salvucci ME, Crafts-Brandner SJ**. **2004**. Relationship between the heat tolerance of
1111 photosynthesis and the thermal stability of Rubisco activase in plants from contrasting thermal
1112 environments. **134**: 1460–1470.

1113 **Salvucci ME, DeRidder BP, Portis AR**. **2006**. Effect of activase level and isoform on the
1114 thermotolerance of photosynthesis in Arabidopsis. *Journal of Experimental Botany* **57**: 3793–
1115 3799.

1116 **Salvucci ME, Osteryoung KW, Crafts-Brandner SJ, Vierling E**. **2001**. Exceptional
1117 Sensitivity of Rubisco Activase to Thermal Denaturation in Vitro and in Vivo. *Plant Physiology*
1118 **127**: 1053–1064.

1119 **Sato H, Mizoi J, Shinozaki K, Yamaguchi-Shinozaki K**. **2024**. Complex plant responses to
1120 drought and heat stress under climate change. *The Plant Journal* **117**: 1873–1892.

1121 **Scafaro AP, Atwell BJ, Muylaert S, Reusel BV, Ruiz GA, Rie JV, Gallé A**. **2018**. A
1122 thermotolerant variant of Rubisco activase from a wild relative improves growth and seed yield
1123 in rice under heat stress. *Frontiers in Plant Science* **9**: 1663.

1124 **Scafaro AP, Bautsoens N, Den Boer B, Rie JV, Gallé A**. **2019a**. A Conserved Sequence
1125 from Heat-Adapted Species Improves Rubisco Activase Thermostability in Wheat 1[OPEN].

1126 **Scafaro AP, Gallé A, Van Rie J, Carmo-Silva E, Salvucci ME, Atwell BJ**. **2016**. Heat
1127 tolerance in a wild *Oryza* species is attributed to maintenance of Rubisco activation by a
1128 thermally stable Rubisco activase ortholog. *New Phytologist* **211**: 899–911.

1129 **Scafaro AP, Posch BC, Evans JR, Farquhar GD, Atkin OK**. **2023**. Rubisco deactivation and
1130 chloroplast electron transport rates co-limit photosynthesis above optimal leaf temperature in
1131 terrestrial plants. *Nature Communications* **14**: 2820.

1132 **Scafaro AP, Vleesschauwer DD, Bautsoens N, Hannah MA, Boer B den, Gallé A, Rie JV**.
1133 **2019b**. A single point mutation in the C-terminal extension of wheat Rubisco activase
1134 dramatically reduces ADP inhibition via enhanced ATP binding affinity. *The Journal of*
1135 *Biological Chemistry* **294**: 17931.

1136 **Serban AJ, Breen IL, Bui HQ, Levitus M, Rebekka Wachter XM, Jez JM**. **2018**. Assembly–
1137 disassembly is coupled to the ATPase cycle of tobacco Rubisco activase. *J. Biol. Chem* **293**:
1138 19451–19465.

1139 **Shivhare D, Mueller-Cajar O**. **2017**. *In vitro* characterization of thermostable CAM Rubisco
1140 activase reveals a Rubisco interacting surface loop. **174**: 1505–1516.

1141 **Shivhare D, Ng J, Tsai Y-CC, Mueller-Cajar O**. **2019**. Probing the rice Rubisco-Rubisco
1142 activase interaction via subunit heterooligomerization. *Proceedings of the National Academy*
1143 *of Sciences of the United States of America* **116**: 24041–24048.

1144 **Song J, Tong G, Chao J, Chung J, Zhang M, Lin W, Zhang T, Bentler PM, Zhu W**. **2023**.
1145 Data driven pathway analysis and forecast of global warming and sea level rise. *Scientific*
1146 *Reports* **13**: 5536.

1147 **Song K, Yim WC, Lee B-M**. **2017**. Expression of heat shock proteins by heat stress in
1148 soybean. *Plant Breeding and Biotechnology* **5**: 344–353.

1149 **Stainbrook SC, Aubuchon LN, Chen A, Johnson E, Si A, Walton L, Ahrendt AJ, Strenkert**
1150 **D, Jez JM**. **2024**. C4 grasses employ distinct strategies to acclimate Rubisco activase to heat
1151 stress. *Bioscience Reports* **44**.

1152 **Stotz M, Mueller-Cajar O, Ciniawsky S, Wendler P, Hartl FU, Bracher A, Hayer-Hartl M**.
1153 **2011**. 1 3 6 6 VOLUME 18 NUMBER 12 DECEMBER 2011 nature structural & molecular
1154 biology. *Nature Structural & Molecular Biology*.

1155 **Taylor T, Denson J-P, Esposito D**. **2017**. Optimizing Expression and Solubility of Proteins in
1156 E. coli Using Modified Media and Induction Parameters. In: Burgess-Brown NA, ed.
1157 Heterologous Gene Expression in E.coli: Methods and Protocols. New York, NY: Springer,
1158 65–82.

1159 **Taylor SH, Gonzalez-Escobar E, Page R, Parry MAJ, Long SP, Carmo-Silva E**. **2022**.
1160 Faster than expected Rubisco deactivation in shade reduces cowpea photosynthetic potential
1161 in variable light conditions. *Nature Plants* **8**: 118–124.

1162 **Waheeda K, Kitchel H, Wang Q, Chiu P-L**. **2023**. Molecular mechanism of Rubisco activase:
1163 Dynamic assembly and Rubisco remodeling. *Frontiers in Molecular Biosciences* **10**: 1125922.

1164 **Wang D, Li X-F, Zhou Z-J, Feng X-P, Yang W-J, Jiang D-A**. **2010**. Two Rubisco activase
1165 isoforms may play different roles in photosynthetic heat acclimation in the rice plant.
1166 *Physiologia Plantarum* **139**: 55–67.

1167 **Warrag MOA, Hall AE**. **1984**. Reproductive responses of cowpea (*Vigna unguiculata* (L.)
1168 Walp.) to heat stress. II. Responses to night air temperature. *Field Crops Research* **8**: 17–33.

1169 **Weber E, Engler C, Gruetzner R, Werner S, Marillonnet S**. **2011**. A modular cloning system
1170 for standardized assembly of multigene constructs. *PLOS ONE* **6**: e16765.

1171 **Werner S, Engler C, Weber E, Gruetzner R, Marillonnet S**. **2012**. Fast track assembly of
1172 multigene constructs using Golden Gate cloning and the MoClo system. *Bioengineered Bugs*
1173 **3**: 38–43.

1174 **Wickham H**. **2017**. Tidyverse: Easily install and load the 'tidyverse'. *R package version* **1**:
1175 2017.

1176 **Wijewardene I, Shen G, Zhang H**. **2021**. Enhancing crop yield by using Rubisco activase to
1177 improve photosynthesis under elevated temperatures. **1**: 2.

1178 **Winter D, Vinegar B, Nahal H, Ammar R, Wilson GV, Provart NJ**. **2007**. An "Electronic
1179 fluorescent pictograph" browser for exploring and analyzing large-scale biological data sets.
1180 *PLOS ONE* **2**: e718.

1181 **Wood SN**. **2017**. *Generalized Additive Models: An Introduction with R, Second Edition*. New
1182 York: Chapman and Hall/CRC.

1183 **Yamori W, von Caemmerer S**. **2009**. Effect of Rubisco activase deficiency on the
1184 temperature response of CO_2 assimilation rate and Rubisco activation state: Insights from
1185 transgenic tobacco with reduced amounts of Rubisco activase. *Plant Physiology* **151**: 2073–
1186 2082.

1187 **Yin Z, Zhang Z, Deng D, Chao M, Gao Q, Wang Y, Yang Z, Bian Y, Hao D, Xu C**. **2014**.
1188 Characterization of Rubisco activase genes in maize: An α-isoform gene functions alongside
1189 a β-isoform gene. *Plant Physiology* **164**: 2096–2106.

1190 **Zahra N, Hafeez MB, Wahid A, Al Masruri MH, Ullah A, Siddique KHM, Farooq M**. **2023**.
1191 Impact of climate change on wheat grain composition and quality. *Journal of the Science of*
1192 *Food and Agriculture* **103**: 2745–2751.

1193 **Zhang N, Kallis RP, Ewy RG, Portis AR**. **2002**. Light modulation of Rubisco in *Arabidopsis*
1194 requires a capacity for redox regulation of the larger Rubisco activase isoform. *Proceedings*
1195 *of the National Academy of Sciences of the United States of America* **99**: 3330–3334.

1196 **Zhang N, Portis AR**. **1999**. Mechanism of light regulation of Rubisco: A specific role for the
1197 larger Rubisco activase isoform involving reductive activation by thioredoxin-f. *Plant Biology*
1198 **96**: 9438–9443.

1199

1200   Supporting Information

1201   **Supporting Information Figures**

1202   Fig. S1. Amino acid residue alignment of the four cowpea Rca isoforms.

1203   Fig. S2. *In vitro* Rubisco reactivation by the four cowpea Rca isoforms.

1204   Fig. S3. Heatwave experimental design and cabinet temperature monitoring.

1205   Fig. S4. Cabinet plant layout design.

1206   Fig. S5. Growth parameters and chlorophyll content during and after heat stress.

1207   Fig. S6. Leaf temperature monitoring over the heatwave experiment.

1208   Fig. S7. T_{crit} calculation from temperature response of chlorophyll fluorescence-derived Fv/Fm.

1209   Fig. S8. Gene expression of heat shock protein 20 (HSP20) and cowpea Rca (RT-qPCR).

1210   Fig. S9. Protocol outline for determination of Rca activity in leaf extracts (LE).

1211   Fig. S10. Specific Rubisco activities of control and heat-treated plants.

1212   Fig. S11. Differential gene expression in heat-treated *versus* control cowpea plants.

1213   Fig. S12. Volcano plots depicting differential gene expression based on log change across the
1214   days of heatwave.

1215   Fig. S13. Potential cis-acting regulatory elements in cowpea Rca promoter regions.

1216   Fig. S14. Protein abundance of Rca isoforms in control and heat-treated plants.

1217   Fig. S15. Rubisco reactivation by the pool of cowpea Rca isoforms in leaf extracts (LE).

1218   **Supporting Information Tables**

1219   Table S1. Reference protein sequences used to identify cowpea Rca genes.

1220   Table S2. Primer sequences for adding Golden Gate overhangs to Rca coding regions.

1221   Table S3. Modelling of the *in vitro* temperature response of ATP hydrolysis and Rubisco
1222   activation by cowpea Rca isoforms.

1223   Table S4. Optimum temperature of in vitro Rubisco activase (Rca) activity.

1224   Table S5. RNA sample QC analysis prior to RNA sequencing.

1225   Table S6. Sequencing and alignment statistics.

1226   Table S7. MIQE checklist for RT-qPCR.

1227   Table S8. RT-qPCR primers.

1228   Table S9. Modelling of the temperature response of Rubisco activation by cowpea Rca in leaf
1229   extracts of control and heat-treat plants.

1230   References